A widespread electrical brain network encodes anxiety in health and depressive states

Dalton N. Hughes[3,*], Michael Hunter Klein[8,*], Kathryn Katsue Walder-Christensen[3], Gwenaëlle E. Thomas[3], Yael Grossman[2], Diana Waters[2], Anna E. Matthews[2], William E. Carson[10], Yassine Filali[7], Mariya Tsyglakova[6], Alexandra Fink[3], Neil M. Gallagher[3], Masiel Perez-Balaguer[2], Colleen A. McClung[6], Jean Mary Zarate[2], Rainbo C. Hultman[7], Stephen D. Mague[2], David E. Carlson[,5,8,9,10,†], Kafui Dzirasa[1,2,3,4,†].

[1]Howard Hughes Medical Institute, Chevy Chase, Maryland 20815, USA; [2]Dept. of Psychiatry and Behavioral Sciences, [3]Dept. of Neurobiology, [4] Dept. of Neurosurgery, [5]Dept. of Biostatistics and Bioinformatics, Duke University Medical Center, Durham, North Carolina 27710, USA; [6]Department of Psychiatry, University of Pittsburgh Medical School, Pittsburgh, PA 15213; [7]Department of Molecular Physiology and Biophysics, Department of Psychiatry, University of Iowa, Iowa City, IA, 52242 USA; [8]Dept. of Electrical and Computer Engineering, [9]Dept. of Civil and Environmental Engineering, [10]Dept. of Biomedical Engineering, Duke University, Durham North Carolina 27708, USA.

*These authors contributed equally

†Senior authors; Contributed equally

Abstract

In rodents, anxiety is charactered by heightened vigilance during low-threat and uncertain situations. Though activity in the frontal cortex and limbic system are fundamental to supporting this internal state, the underlying network architecture that integrates activity across brain regions to encode anxiety across animals and paradigms remains unclear. Here, we utilize parallel electrical recordings in freely behaving mice, translational paradigms known to induce anxiety, and machine learning to discover a multi-region network that encodes the anxious brain-state. The network is composed of circuits widely implicated in anxiety behavior, it generalizes across many behavioral contexts that induce anxiety, and it fails to encode multiple behavioral contexts that do not. Strikingly, the activity of this network is also principally altered in two mouse models of depression. Thus, we establish a network-level process whereby the brain encodes anxiety in health and disease.

Keywords

Anxiety, brain networks, dynamics, limbic, depression, and stress.

Introduction

Anxiety is a mental state marked by heightened pressure, concern, or apprehension related to uncertain future circumstances [1]. The anxious state can be adaptive to increase the rate of survival, or it can become overly generalized and persistent in a manner that yields behavioral pathology that can lead to anxiety disorders. These disorders constitute the largest group of mental disorders in Western and high-income societies, with nearly 34% of U.S. adults directly impacted in their lifetime [1, 2]. Strikingly, the prevalence of symptoms of anxiety disorders or other mental health disorders had increased during the height of the COVID-19 pandemic [3]. As such, it is imperative to discover the biological basis of the anxious brain state and to delineate how the brain encodes anxiety in the disordered state.

Non-invasive human imaging studies have demonstrated altered activity in multiple cortical and limbic brain regions, including the amygdala, prefrontal cortex, and hippocampus during heightened anxiety and synchronized activity between these regions and others at the milliseconds to seconds timescales [4-7]. Human intracranial recordings have also demonstrated altered coherence in networks with some of these regions linked to higher trait anxiety [8], pointing towards the involvement of integrated multi-regional circuits in mediating the anxiety state.

A myriad of rodent studies has implicated homologous regions in mediating anxiety: the amygdala (Amy), ventral hippocampus (Hip), and subregions of the prefrontal cortex (PFC). Pharmacological lesions and optogenetic inactivation studies have implicated the necessity of these brain regions for anxious behaviors [9, 10]. Furthermore, precise circuit-level studies in rodent models have further delineated the role of these brain regions and their integrated circuits [11]. For example, millisecond-level synchrony is observed in the mPFC, Amy and/or Hip during key aspects of anxiety-related behaviors [12-17], and optogenetic interrogation of projections involving these regions modulate anxiety-related behaviors [18-23]. Yet it remains to be clarified how these circuits reliably integrate across timescales (i.e., network-level stability) to selectively encode anxiety across animals and behavioral contexts (i.e., generalization) in healthy animals and in disease states.

Because LFPs capture generalized patterns of neural activity that can be consistently sampled across subjects [24], we previously developed a machine learning technique called discriminative Cross-Spectral Factor Analysis-Nonnegative Matrix Factorization (dCFSA-NMF) to discover behaviorally relevant ensembles of LFP activity that synchronize at both the milliseconds and seconds timescale (i.e., electrical functional connectome -electome - networks). An electome network can be composed by LFP oscillatory power from each brain area, millisecond-resolution coherence between oscillations from pairs of brain regions, and/or directional oscillations (an indication of information transfer between pairs of brain regions assessed using Granger causality testing), ranging from 1-56Hz. Moreover, dCSFA-NMF was designed to discover electome networks that encode behaviorally relevant internal states both within and across mice [25-27]. Here, we used dCSFA-NMF to discover a distinct electome network that selectively encodes normal anxiety across multiple contexts, and anxiety dysfunction in mouse models of psychiatric disorders.

Results

Distributed electome networks encode a convergent anxious internal state

Forty-one male mice were implanted with multiwire electrodes to concurrently target prefrontal cortex (cingulate, prelimbic and infralimbic cortex), amygdala, ventral hippocampus, nucleus accumbens, medial dorsal thalamus, and ventral tegmental area (VTA). Following their recovery, we employed a two-stage approach to discover how distributed neural activity encodes an internal state for anxiety. First, we utilized a translational anxiogenic protocol based on treatment with the antidepressant

fluoxetine, which has been shown to induce anxiety-like behavior in mice [28], versus a control saline condition (see also Supplemental Figure S1). Second, we tested whether the electome networks learned for this paradigm also encoded the internal state induced by two other anxiogenic paradigms: the elevated plus maze (EPM) and the bright open field (BOF). The amount of time a mouse spends within exposed regions of these assays (open arms in the EPM and center of the BOF) is used to infer anxious internal states. As mice with the highest anxiety-like behavior may never enter the exposed regions of these assays, we modeled anxiety as the internal state that was causally induced by the three paradigms (Fig. 1A). We trained our network model at one-second resolution to enable us to compare network activity to on-going behaviors widely utilized to assess the anxiety state of mice [12, 29]. The 41 implanted male mice were exposed to 1 of the 3 experimental paradigms (17 mice were subjected to two paradigms).

Our dCSFA-NMF model trained on the neural data acquired during the fluoxetine paradigm successfully distinguished the low and high anxiety states (saline and fluoxetine treatment, respectively) in newly implanted C57 mice that had not been used to train the model (Mann Whitney AUC = 0.68 ± 0.01; Fig. 1B, see also Supplemental Figure S2); however, the model failed to distinguish low and high anxiety states when it was tested on data obtained from the other two paradigms (AUC = 0.49 ± 0.01 and 0.44 ± 0.01 for EPM and BOF, respectively). We also found that dCSFA-NMF models trained on the EPM or BOF assay similarly failed to distinguish the low and high anxiety states of the fluoxetine assay. These analyses employed four-fold cross-validation with 3-7 hold out mice within assay per fold, and 9-26 hold out mice between assay per fold. A full discussion of the dCSFA-NMF model training procedure and hyperparameter selection can be found in the Methods section.

After failing to discover a generalized internal state for anxiety solely using training data from one paradigm, we took inspiration from multi-task learning [30] and adapted dCSFA-NMF for training on multiple assays jointly (Fig. 1C). Specifically, the multi-assay dCSFA-NMF model utilized training data from all three contexts (FLX, EPM, BOF) to discover an electome network that was shared between them. Though we successfully discovered such a shared electome network, we also found that small permutations of the animal assignments between training and validation data groups yielded electome networks composed of different LFP spectral features (Fig. 1D) while remaining predictive of the anxiety paradigms.

To address this lack of stability, we developed and employed a cosine similarity-based metric for evaluating network stability across multiple training permutations. For this metric, a low cosine distance reflects electome network consistency. We then systematically increased the number of supervised networks in our dCFSA-NFM model, utilizing all supervised networks in a joint prediction logistic regression framework, and quantified the stability of the resultant electome networks. With this approach, we found that a model trained with three supervised electome networks optimally balanced simplicity and electome network stability across multiple runs on perturbated and partitioned training data (Supplemental Figure S3). This multi-network model encoded the anxiety state across all three assays in the same seventeen new mice used in testing of the single-assay trained models (AUC = 0.59 ± 0.04, 0.76 ± 0.03, and 0.84 ± 0.03 for FLX, EPM, and BOF, respectively; Fig 1E). Critically, no individual brain region, or pair of regions, independently encoded an anxiety state shared by all three paradigms (Fig 1F, see also Supplemental Figure S4). Thus, our findings argued that the anxiety brain state was encoded at the multi-region level.

Two electome networks independently encode the anxious internal state

The three supervised networks that jointly predicted the anxiety state contributed 26%, 73%, and 1% of the joint logistic regression model prediction probability, averaged across assays (heretofore referred to as Electome Networks 1, 2 and 3, respectively; see Fig. 2D). Electome Network 1 was comprised by prominent beta (14-30) and gamma oscillations (30-55Hz) that led from VTA, amygdala, and medial dorsal thalamus, and converge in infralimbic cortex and nucleus accumbens. Electome Network 2 was comprised of prominent beta and gamma oscillations that led from prelimbic cortex, relayed through medial dorsal thalamus, and converged in the amygdala. Electome Network 3 was represented by synchronized theta oscillations (4-11Hz) across many of the regions we probed (Fig. 2A-C, see also Supplemental Figure S5-7). Thus, the three electome networks were each represented by distinct ensembles of LFP activity.

Importantly, the electome networks included circuits previously implicated in aspects of anxiety-like behavior in the broader literature. For example, optogenetic stimulation of the amygdala→infralimbic cortex circuit, a component of Electome Network 1, has been shown to increase anxiety-behavior during the EPM and BOF in mice [19]. Mouse studies have described increased activity in the ventral hippocampus→prefrontal cortex circuit in the EPM and BOF [12, 13], and causal stimulation of this circuit increases anxiety behavior [22]. Increased synchrony between amygdala and ventral hippocampus has been implicated in trait and state anxiety in human intracranial recording experiments [8] and in mediating EPM anxiety behavior in causal mouse experiments [31]. Such circuits are prominently featured in Electome Network 2. Finally, increased IL activity, as featured in Electome Network 2 and 3, drives anxiety behaviors in mice in the EPM [32]. Thus, many circuits proposed previously shown to encode aspects of anxiety were featured in our discovered electome networks.

Though our goal was to discover at least one electome network that was shared across the three anxiety paradigms, our multi-supervised network learning strategy had the potential to discover three electome networks for which each solely encoded one of the three assays. Thus, to ensure that we had indeed discovered an electome network that generalized across anxiety paradigms, we tested whether Electome Network 1, 2 or 3 encoded the anxious state in all three paradigms, again in the seventeen new mice. Electome Network 1 and 2 both independently generalized to all three paradigms ($P<0.05$ for all comparisons against a null distribution using a one-sided Mann-Whitney U test) while Electome Network 3 only encoded the internal state induced by the BOF assay ($P = 1$, $P=0.66$; $P <0.05$ for FLX, EPM, and BOF, respectively; Fig 2D). Given that only Electome Network 1 and 2 independently encoded all three assays, and Electome Network 3 only contributed 1% to multi-network prediction, we limited our subsequent analysis to Electome Network 1 and 2. Critically, we also verified that Electome Networks 1 and 2 generalized to female mice when we compared their activity in the home cage to the EPM (AUC=0.63±0.05, $U=5$, $P=0.039$; AUC=0.65±0.06, $U=4$, $P= 0.027$ for Electome Networks 1 and 2, respectively, using a one-sided paired Wilcoxon sign rank test; N=8 female mice)

Electome Network activity encodes features of anxiety-related paradigms.

We further validated Electome Network 1 and Electome Network 2 of our multi-assay trained model by examining network activity dynamics during various anxiogenic events both within the training assays (i.e., FLX, EPM, and BOF) and in new experimental contexts to control for confounding emotional states. All analyses were performed on new subjects not used in model training.

Within the FLX training assay, we observed that the activity of Electome Networks 1 and 2 decreased across the neural recording period in the saline and fluoxetine treated mice ($F_{59,295}=4.05$, $P=0.014$ and $F_{59,295}=3.85$, $P=0.015$ for time effect across minutes for Electome Network 1 and 2 activity, respectively,

using two-way ANOVA with correction). No differences were observed in this effect across the treatments ($F_{59,295}$=1.14, P=0.37 and $F_{59,295}$=1.36, P=0.28 for treatment × time interaction effect, for Electome Network 1 and 2 activity, respectively, using two-way ANOVA with correction; see Fig. 3A). Thus, activity in both networks decreased as mice habituated following the experimental injections, providing additional evidence that the networks tracked the internal anxiety state of the mice.

To further explore whether network activity habituated following other anxiogenic stimuli, we also analyzed network activity in the EPM and BOF, relative to the activity observed in the home cage. We focused our analysis on periods during which mice were in the closed arms of the EPM or the periphery of the BOF, since these are considered the safe zones of the assays. This analysis approach also enabled us to control changes in network activity that may be location specific. Activity in both networks increased sharply after the mice were first placed in the behavioral area, and then habituated across the remaining of the 5-minute testing session (Fig. 3B; T=-11.246, P<0.001; T=-11.116, P<0.001, for time effect for Network 1 and 2, respectively, using an ANCOVA). Thus, network activity in both assays paralleled the response we observed in the fluoxetine assay. Next, we tested whether activity in the networks was behaviorally relevant. Specifically, since we found that the BOF induced a higher network activity than the EPM (Fig. 3B; T=14.036, P<0.001; T=13.248, P<0.001, for assay effect for Network 1 and 2, respectively, using an ANCOVA), we analyzed the behavioral profiles of mice in both assays to determine whether the BOF induced greater anxiety-related behavioral avoidance. After verifying that the mice spent substantially more time in the safe zones vs. anxiogenic zones in both assays (T_{10}=19.9; $P<10^{-8}$ and T_8=29.8; $P<10^{-8}$, for EPM and BOF, respectively, using a one-tailed paired t-test, Fig. 3C), we quantified the bout length when animals entered the anxiogenic zones. We found that the length of each bout in the center zone of the BOF was significantly shorter than the bout length in the open arm for the EPM (T_{18}= 2.6; P=0.009, using a one-tailed unpaired t-test, Fig. 3C), demonstrating that the mice exposed to the BOF showed higher anxiety-related avoidance.

Network 2 activity, but not Network 1, showed much stronger habituation between the initial and latter segments of the BOF, compared to the EPM (U=33 and P=0.11; U=27 and P=0.047, for Network 1 and 2, respectively, using a one-sided Mann-Whitney U test; Fig. 3D). Consistent with this observation, we found that mice avoided the center of the BOF more during the first half of the assay (T_8=3.97 and P=0.004 using a two-tailed paired t-test; see Fig. 3F). In contrast, no such behavioral pattern was observed in the EPM (Fig. 3E). Here, mice showed large variability in when they occupied the open arms across the testing session (T_{10}=0.70 and P=0.50 using a two-tailed paired t-test). Taken together, these results showed that mice were least likely to occupy the anxiogenic zone under the experimental context which produced the highest Network 2 activity (first half of the BOF). Thus, Network 2 activity broadly encoded the anxiety-related behavioral differences observed across the assays.

Next, we tested whether network activity encoded behavior on a moment-to-moment basis within the assays. Specifically, we reasoned that three distinct patterns of anxiety could intersect with behavior: 1) Mice might show higher anxiety when they are in the anxiogenic zones of the assay. 2) The anxiogenic zones of the assay might induce a feeling of anxiety that peaks several seconds later irrespective of the animal's future location and 3) high anxiety might preclude mice from entering the anxiogenic zones [31]. Thus, we set out to determine whether the two networks showed activity consistent with any of these 3 patterns. Importantly, though all data recorded during the EPM and BOF assays were used to discover our putative anxiety networks, the moment-by-moment location of the mice in the EPM and BOF (anxiogenic vs. safe zone) was not. Thus, our training approach enabled an unbiased assessment of their activity related to ongoing anxiety behavior. For our analysis, we first isolated all the one-second

intervals when mice were in the open or closed arm of the EPM. We also isolated neural activity up to five seconds following these timepoints, and up to five seconds prior to these timepoints [15, 31].

Both networks failed to encode whether mice were in the open or closed arms of the EPM (U=42 and P=0.23; U=41 and P=0.26; for Network 1 and 2, respectively, using a one-sided paired Wilcoxon sign rank test; Fig. 3G). On the other hand, we found that Network 2 activity (U=61 and P=0.0049 using a one-sided paired Wilcoxon sign rank test), but not Network 1 (U=19 and P=0.90 using a one-sided paired Wilcoxon sign rank test), was higher in the five seconds interval following the open arm location of mice (regardless of whether they returned to the closed arm during this period). Thus, an increase in Network 2 activity was induced by the anxiogenic zone of the assay, providing support for the second pattern of anxiety listed above. Neither Network 1 or 2 activity was lower in the 5-second interval preceding the open arm location (regardless of the location of the mouse during this interval), compared to activity preceding the closed arm of the EPM (U=46 and P=0.88; U=27 and P=0.32 for Network 1 and 2, respectively, using a one-sided paired Wilcoxon sign rank test Fig. 3G). This failed to support the third pattern of anxiety for which high network activity might preclude entrance into anxiogenic zones. Though Network 1 and 2 also failed to encode whether mice were in the center or periphery of the BOF (U=22 and P=0.54, U=20 and P=0.63 using a one-sided paired Wilcoxon sign rank test), we found that both Networks showed lower center activity within the preceding 5 seconds interval compared to the periphery (U=7 and P=0.037; U=8 and P=0.049, using a one-sided paired Wilcoxon sign rank test, Fig. 3H). Together, these findings showed that high activity in either network predicted that mice would be in the safe zone of the BOF in the future, thus supporting the third pattern of anxiety. No increases in Network 1 or 2 activity were observed in the 5-second interval following the center location compared to either network's activity when mice were in the periphery in the BOF (U=18 and P=0.71, U=13 and P=0.88 using a one-sided paired Wilcoxon sign rank test). Overall, these results showed that Network 2 activity was increased by the open arms of the EPM, while high activity in both Networks precluded mice from entering the center zone in the BOF. This latter pattern of activity was consistent with our observation that mice occupied the center zone less during the first half of the BOF when activity in both networks was highest. Thus, Network 1 and 2 activity was behaviorally relevant and supported our three patterns of anxiety, though the pattern for which anxiety behavior was encoded by these networks varied between the two assays.

Electome Network activity does not encode arousal

As anxiety is correlated with arousal, our training approach could plausibly discover networks that reflect an arousal state rather than anxiety. To explore this possibility, we used data acquired from two independent assays that are thought to increase arousal but not anxiety. During these assays, data was collected from the same brain regions used initially for model training, and LFP activity was projected into the previously learned multi-assay trained model to calculate the activity of Electome Network 1 and 2 for each second. In the first assay, mice were trained to maintain a nose poke for 5 seconds. Tones of decreasing pitch were played throughout the 5-second trial, and a 5µL sucrose reward was delivered at the end if mice remain in the port for the entire 5 seconds. When we tested whether reward delivery increases electome network activity, we failed to identify a significant response in either network (U=30 and P=0.82; and U=41 and P=0.99, for Electome Network 1 and 2 activity, respectively, using a one-sided paired Wilcoxon sign rank test; Fig 4A). Next, we quantified Electome Network 1 and 2 activity responses during a classic social preference assay, where mice freely explore an object and a novel social stimulus mouse housed at the two ends of a chamber. Here, the social stimulus mouse is considered both arousing and rewarding, as experimental mice generally choose to spend more time with the other mouse than the object, and social encounters activate reward circuitry [33]. We failed to discover increases in Electome Network 1 or 2 activity during interactions with the stimulus mouse, compared to

the inanimate object (U=60 and P=0.95; U=47 and P=0.74, for Electome Network 1 and 2 activity, respectively, using a one-tailed paired Wilcoxon sign rank test, Fig. 4B). These results demonstrate that both networks fail to encode arousal as no increase in network activity is observed during either the trained or innate reward assays.

Electome Network activity encodes the internal state induced by additional anxiety paradigms

We further probed whether our electome networks encode a robust anxiety-related brain state using additional paradigms that induce anxiety in a manner that is distinct from our initial assays. Again, all analyses were performed on new mice that were not used during model training. We first examined network activity during direct optogenetic stimulation neurons in the ventral hippocampus. This region has been causally implicated in anxiety-related behaviors in rodents [34], and it was a critical upstream node in one of our networks. Moreover, we selectively stimulated the subset of neurons that projected to lateral hypothalamus since the ventral hippocampus→ lateral hypothalamus circuit had been shown to drive anxiety-related avoidance in the EPM and BOF [20]. Mice were infected with an adenoassociated virus (AAV) to express Channelrhodopsin-2 using (ChR2) in the ventral hippocampus and implanted with microwires to target the same regions utilized to learn our multi-assay trained electome network. A microwire and optic stimulating fiber was also implanted in lateral hypothalamus, concurrently (Fig. 5A). Mice were then stimulated with blue light to activate ChR2, or yellow light as a negative control, while neural activity was recorded in their home cage. As expected, blue light induced local and remote LFP activity, while yellow light did not (Fig 5B). When we projected neural activity recorded during these stimulations into our learned multi-assay trained model, we found that ventral hippocampus → lateral hypothalamus stimulation increased Electome Network 2, but not Electome Network 1 activity (U=20 and P=0.14; U=0 and P<0.001, for Electome Network 1 and 2 activity, respectively, using a one-sided paired Wilcoxon sign rank test, Fig. 5C and 5D). Thus, these data further validated Electome Network 2 as a network-level code for the anxious internal state.

We subsequently examined whether Electome Network 1 or 2 encode the internal state induced by fear conditioning. In this classic paradigm, mice are exposed to seven repeated auditory cues, each paired to a foot shock (conditioned stimulus, CS+). On a subsequent recall session, conditioned mice exposed to the auditory cue in the absence of the foot shock typically exhibit a freezing response. For our conditioning paradigm, we substituted the foot shock with a high-pressure air puff during conditioning (Fig. 5E). This enabled us to minimize electrical noise during LFP recording. Mice exposed to our modified air puff stimulus treated mice (CS+) exhibited increased freezing behaviors during the recall period when compared to controls (CS-) (U=21 and P=2.3×10^{-4} using a one-sided Mann-Whitney U test; Fig. 5F).

We compared electome network activity between CS+ and CS- mice at the final stimulus of the aversive conditioning (i.e., the 7th tone). Though we observed a trend in Electome Network 1 activity, neither Electome Network 1 or 2 were significantly elevated in CS+ mice during the brief interval immediately prior to the tone, compared to the CS- mice (U=105 and P=0.051; and U=78 and P=0.45, for Electome Network 1 and 2, respectively, using a one-sided Mann-Whitney U test, Fig. 5G, 5H). Conversely, Electome Network 2, but not Electome Network 1, activity was significantly higher in CS+ mice during the brief interval immediately after the presentation of the tone (U=100 and P=0.09; and U=110 and P=0.028, for Electome Network 1 and 2 respectively, using a one-sided Mann-Whitney U test, Fig. 5I, 5J). Importantly, our post-hoc analysis found no difference in Electome Network 1 or 2 activity prior to, or, immediately following the first tone exposure (see Supplemental Figure S8). As such, Electome Network 2 encodes an acute state generated by the presentation of a threat-paired stimulus. Overall, Electome Network 2 encodes a behaviorally relevant component of the classic fear conditioning paradigm, while

Electome Network 1 showed a trend towards encoding a more generalized state that emerged with fear conditioning.

Finally, having discovered that Electome 2 encoded anxiety features of our fear conditioning paradigm, but not arousal or reward, we asked whether either network broadly encoded an acute negative experience. Specifically, while anxiety is a negative affective state, not all negative experiences produce anxiety. Thus, we further probed our fear conditioning paradigm data to test whether the activity in our electome networks increased acutely during an ongoing negative experience. We reasoned that prior to conditioning, the first air puff should immediately invoke negative affect, but not anxiety. As such, we quantified electome network activity in the CS+ mice while they experienced the first air puff and compared that to neural activity from the CS- mice, which did not receive an air-puff. Using this approach, we found that the air puff acutely increased Electome Network 1, but not Electome Network 2, activity (U=118 and P=0.009; and U=86 and P=0.28, for Electome Network 1 and 2, respectively, using a one-sided Mann-Whitney U test, Fig. 5K, 5L; see also Supplemental Figure S8). These results indicated that Electome Network 2 activity was specific for anxiety, while Network 1 was not.

Electome Network activity is altered in mouse models of mood disorders

Anxiety behavior is altered in mood disorders. Indeed, bipolar mania is characterized by impulsivity and risk taking[35] (reflective of decreased anxiety processing), while major depressive disorder is highly co-morbid high anxiety[36]. We reasoned that a causal manipulation that induces a manic-like state in mice should suppress network activity when mice were placed in a context where network activity should otherwise be high. Similarly, we reasoned that causal manipulations that induce a depression-like state should increase network activity when mice were placed in a context where network activity should otherwise be low. Thus, we quantified Electome Network 1 or 2 activity in a mouse model of mania and two of the most widely utilized mouse models for major depressive disorder.

The *ClockΔ19* mouse line has been proposed as a model of bipolar mania [37]. These mice have a point mutation in the circadian gene *Clock* and exhibit altered circadian rhythms, hyperactivity, increased reward drive, and decreased anxiety-related behavior [15, 37, 38]. Moreover, many cellular, neurophysiological, and behavioral alterations in these mutant mice are normalized by chronic lithium or valproic acid treatment [37, 39, 40], providing further validation for the *ClockΔ19* mouse as a model of bipolar mania. After confirming that *ClockΔ19* mice demonstrate diminished anxiety behavior in the EPM ($T_{1,32}$=2.9; P=0.003 using unpaired t-test, Fig. 6A), we implanted male and female *ClockΔ19* mice and their wild-type littermate controls with microwires targeting the same brain regions used to learn our electome networks. We then quantified neural activity while mice were in the home cage and on the EPM. Exposure to the EPM induced Network 1 activity in both genotypes ($F_{1,19}$ = 15.81 and P =8.08×10^{-4} for assay effect using mixed-effects model ANOVA; U=2 and P=0.003, U=10 and P=0.02, for wild type and *ClockΔ19* mice, respectively using one-tailed Wilcoxon sign rank test). Similarly, exposure to the EPM induced Network 2 activity in both genotypes as well ($F_{1,19}$ = 17.17 and P = 5.51×10^{-4} for assay effect using mixed-effects model ANOVA; U=4 and P=0.068, U=9 and P=0.016, for wild type and *ClockΔ19* mice, respectively, using a one-tailed Wilcoxon sign rank test sign rank test). We further probed neural activity across genotypes in the otherwise high-anxiety context (i.e., the EPM). For this analysis, we isolated intervals when mice were in the closed arms, an approach which enabled us to isolate neurophysiological differences that result by disruption of the CLOCK gene, while controlling for the altered behavioral profiles displayed by the mutants. When we compared network activity in closed arms of the EPM across genotypes, we observed lower Network 1 and 2 activity in the *ClockΔ19* mice compared to their littermate controls (T=10.97, P<0.001, Network 1; T=-7.42, P<0.001, for genotype effect for Network 1 and 2, respectively, using an ANCOVA, Fig. 6B). Thus, a genetic manipulation used to

model bipolar mania (and thus decrease anxiety-related behavior) in mice was sufficient to reduce Electome Network 1 and 2 activity in an otherwise angiogenic context.

Next, we explored network activity in two depression models that causally induce anxiety-related behavior. In the chronic social defeat stress paradigm, mice are repeatedly exposed to larger-aggressive mice. After 10 such exposures, a subset of mice, classically referred to as *susceptible*, exhibit social avoidance, disrupted reward behavior, and anxiety-like behavior [41, 42]. Conversely, the other subset of mice, termed *resilient*, exhibit normal social and reward behavior [41, 42] (Fig. 6C-D). Interestingly, despite the well-described differences in appetitive behavior, prior work has reported the emergence of anxiety-like behavior in both the susceptible and resilient mice [41, 43]. Indeed, we find that exposure to chronic social defeat stress induces open arm avoidance in the EPM for both susceptible and resilient mice uniformly (t_{20}=2.27 and P=0.02, for comparison between stress and unstressed mice using a one-tailed Welch's t-test; t_{10}=0.16 and P=0.87 for post-hoc comparison between susceptible and resilient mice; see Fig. 6E). Therefore, we quantified whether this stress paradigm also increased Electome Network 1 or 2 activity in both the susceptible and resilient groups compared to non-stressed controls. Since we reasoned that stress exposure should induce a persistent anxious internal state, we probed activity recorded while animals were alone in their home cage. Though chronic social defeat stress exposure failed to induce Electome Network 1 activity (U=468 and P=0.90 using one-sided Mann-Whitney U test), we found significantly higher Electome Network 2 activity in the stressed mice (U=151 and P<0.01 using one-sided Mann-Whitney U test, Fig. 6F, left). Moreover, no difference in Electome Network 2 activity was observed between susceptible and resilient mice (U=382 and P=0.62, for post-hoc analysis using a two-sided Mann-Whitney U test, Fig. 6F, right). Thus, chronic social defeat stress induced anxiety-like behavior and increased Electome Network 2 activity in both groups, despite differences in how stress impacted their reward function.

We next quantified network activity in mice exposed to chronic mild unpredictable stress. In this paradigm, mice are repeatedly exposed to a series of stressors over eight weeks. Specifically, test mice are subjected to two stressors per day, one occurring during the light phase of their circadian rhythm cycle and the other during the dark phase. Stressors, including environmental stressors, food/water restriction, or physical restraint, were chosen according to a pseudo-random schedule. Exposure to this protocol induces altered reward and social behavior, as well as increased anxiety-related behavior in mice compared to their non-stress controls [44, 45]. After verifying that chronic mild unpredictable stress induced open arm avoidance in the EPM (t_{19}=2.37 and P=0.018, for comparison between stress and unstressed mice using a one-tailed Welch's t-test; see Fig. 6G), we quantified electome network activity in stressed mice and non-stressed controls, again in their home cage. Like chronic social defeat stress, exposure to chronic mild unpredictable stress increased Electome Network 2 activity (U=81 and P=0.036, using a one-sided Mann-Whitney U test, Fig. 6H, left). Thus, two of the most widely utilized paradigms for modeling depression in mice converged on a common network-level signature. Interestingly, chronic mild unpredictable stress also increased Electome Network 1 activity as well (U=82 and P=0.031, using a one-sided Mann-Whitney U test, Fig. 6H, right), demonstrating an even broader impact of this stress paradigm on anxiety-related neural activity.

Discussion

Preclinical models have played a role in the development of therapeutics for emotional disorders. These efforts would be greatly enhanced by the discovery of biological mechanisms that instantiate affective internal states in health and disease, and any such mechanisms must generalize across both animals and contexts to achieve their true translational potential. Here, we employed multisite electrical recordings

in freely behaving mice subjected to a collection of behavioral and experimental paradigms to discover and validate an electome network that encoded such a generalized anxious internal state. We reasoned that a putative anxious internal state could be observed at the intersection of many distinct paradigms used to model and induce anxiety behavior. Moreover, we reasoned that the unique features of these paradigms would enable us to disambiguate this anxious internal state from other internal states such as arousal and positive affect (i.e., reward state), or other task relevant variables (Fig. 7A). Machine learning models trained solely using data from one anxiety paradigm failed to generalize to other paradigms. On the other hand, a model trained using data from three assays discovered a network reflecting a shared internal anxious state. Specifically, this electome network generalized to additional anxiety paradigms, including direct optogenetic interrogation of cells originating from a key network node and a classic fear conditioning assay, highlighting its sensitivity. Finally, the electome network failed to encode multiple behavioral assays that induce rewarding and/or arousing (but not anxious) internal states, demonstrating its specificity (Fig. 7B). Thus, our multi-assay learning approach discovered a generalized anxious brain state.

While each of our initial three paradigms could be encoded by at least one implanted region, no single brain region could independently encode an internal state shared across the three paradigms. Moreover, we were unable to capture a signature for a shared anxiety state when we trained models using the predictors from pairs of regions (power across both regions, and the coherence and Granger coherence measures between them). Strikingly, this approach even failed for pairs of regions that had been previously shown to synchronize during anxious states in the EPM. This suggests that activity within a given brain region or circuit captures some behavioral/affective features of each individual assay, while failing to independently encode a generalized anxiety state. For example, activity in a region/circuit may encode non-specific neural responses to the induction paradigms (e.g., sensing a bright light, or non-specific drug effects), or behavioral features that correspond with anxiety in one of the three assays (e.g., locomotion). Because we employed different anxiety induction protocols (bright light vs. drug injection) and behavioral contexts (open lit area vs. home cage), we encouraged our machine learning strategy to discover a generalized anxiety state rather than specific features of each assay. Therefore, we assert that while each individual region contains assay-relevant information, the anxious brain state is optimally represented at the network-level, where activity across many distinct brain regions/circuits is integrated at the sub-seconds timescale. Taken together, our findings highlight two important principles to help discover the neural architecture underlying affective states: 1) employ multiple distinct paradigms to discover generalized affective states rather than features of an assay, and 2) utilizing neural activity acquired from multiple brain regions [24].

We do not contend that the learned electome network provides a comprehensive description of the anxious internal state. Rather, we believe that this state is also coupled to physiological changes across brain regions involved in sensory and motor function, and throughout the body. It is also likely that several neural circuits outside of Electome Network 2 can converge to impact its activity. Indeed, we found that stimulating ventral hippocampal projections in lateral hypothalamus increased Electome Network 2 activity. Thus, we assert Electome Network 2 provides a robust and objective measure of the internal state that mediates anxious behavior, enabling future preclinical studies to dissect and regulate neural processes that contribute to anxiety in disease states.

Interestingly, when we probed the response of the Electome Networks 1 and 2 to an acute air puff, we found that only Electome Network 1 responded to this noxious stimulus. While this observation established that Electome Network 2 was specific for encoding an anxious internal state, it raises the hypothesis that Electome Network 1 may broadly encode a negative affective state.

Multiple patterns identified by our analysis provided support such an interpretation. Specifically, though our analysis strategy employed one-tailed statistical tests, we observed several instances where network activity tended to respond in the opposite direction (i.e., P>0.95). Indeed, while our appetitive behavioral paradigms failed to induce activity in Electome Network 1 or 2, we observed that Electome Network 1 tended to show a graded decrease in activity during behavioral periods consistent with reward anticipation (Fig. 4A, left) and during interaction with an appetitive social stimulus (Fig. 4B, left). When we quantified neural activity when mice were in the open arm of the mice, we observed that Network 1 activity tended to be elevated in the preceding 5 second interval. Moreover, this activity tended to decrease across during this interval (Fig. 3G). Such a pattern in network activity was not observed for Network 2, nor was it observed in the interval preceding when mice were in the closed arm for either network.

This putative decrease in Electome Network 1 activity may reflect an internal process whereby animals briefly suppress a negative affective/avoidance network, enabling them to approach an aversive context or one that carries perceived risk. This interpretation is supported by our findings in the *ClockΔ19* mice which model a manic-like state. Mania is characterized by increased impulsivity and risk taking, and this genetic strain exhibited decreased anxiety-related behavior. We found decreased Electome Network 1 activity in the *ClockΔ19* mouse when they were in a context that should otherwise induce anxiety. Taken together, these raise the idea that Electome Network 1 and 2 cooperate to shape behavior related to anxiety. In this putative framework, Electome Network 2 encodes anxiety, while Electome Network 1 shapes behavior outcomes in response to the internal anxiety state and other negative affective states (Fig. 7B). Future experiments will be necessary to test the validity of this putative framework.

Though Electome Network 2 failed to show increased activity in response to an acute negative stimulus, as Electome Network 1 had, we observed that Electome Network 2 activity tended to decrease after sucrose reward delivery (P>0.95 using one-tailed analysis; Fig. 4A, right). These findings raise the intriguing potential that anxious and negative internal states may counterbalance the appetitive internal state. Indeed, depression is characterized by disrupted appetitive drive and high anxiety, while bipolar mania is characterized by high appetite drive and disrupted anxiety. Supporting the translational utility of Electome Network 2, we quantified its activity in a mouse model of mania and two well established preclinical animal models of depression based on chronic stress exposure. The mouse model of mania exhibits predictive validity as it shows increased reward drive and decreased anxiety-like behavior that responds to chronic lithium treatment [37]. Similarly, both stress models exhibit predictive validity with depression as they produce a heightened anxiety-like behavior and an anhedonia phenotype that responds to chronic antidepressant administration [42, 46, 47]. We found decreased activity in Electome Network 2 in the mouse model of mania when mice were in an otherwise high anxiety context (i.e., in the EPM). Conversely, we found increased activity in Electome Network 2 in the depression models. Strikingly, this increased activity was observed when mice were in an otherwise low anxiety context (i.e., in their home cage).

The two depression models showed distinct network changes in Electome Network 1. Exposure to chronic mild unpredictable stress induced Electome Network 1 activity, while exposure to chronic social defeat stress did not. These findings raise the intriguing potential that chronic mild unpredictable stress may more broadly induce a negative affective state, while chronic social defeat stress primarily impacts the anxiety internal state. Future studies to further validate the role of Electome Network 1 in behavior may further clarify the behavioral distinctions between the two depression models. Taken together, our findings establish a brain electome network that encodes anxiety-behavior in health and in disease

models. Moreover, we establish a putative preclinical biomarker for the development of anxiolytic therapeutics.

Figure Legends

Figure 1: Distributed electome networks encodes anxiety states across multiple anxiety-related paradigms. A) Local field potential oscillations recorded from 8 brain regions, concurrently, as mice were subjected to three distinct paradigms used to model anxiety. **B)** dCSFA-NMF results when the network model was used to discover an electome network for each anxiety paradigm. Electome networks learned for the three anxiety paradigms were applied to new mice subjected to the three paradigms (N= 13, 26, and 19 training mice for FLX, EPM and BOF, respectively, and N= 6, 11, 9 holdout mice for FLX, EPM and BOF, respectively). Nine generalization tests for each of the three learned networks were run in new mice subjected to the three different anxiety paradigms. **C)** Multi-assay dCSFA-NMF model used to discover a joint set of electome networks shared across the three anxiety paradigms. **D)** Network Consistency was evaluated by training the dCSFA-NMF model multiple times, where the mice used for training and validation were shuffled. A cosine distance metric quantified the consistency of the supervised networks across runs, where a lower cosine distance reflected greater network consistency. **E)** Box and whisker plots show generalization tests for which the networks learned from the multi-assay dCSFA-NMF model were applied to new mice (same as Fig. 1B) subjected to the three different anxiety paradigms. Dashed line at AUC = 0.5 corresponds to models with no predictive utility. **F)** Predictive utility of multi-region multi-assay dCSFA-NMF network model (same as Fig. 1E) vs. models solely based on activity from single brain regions. Models that showed significant encoding are highlighted in pink (data analyzed using a single-sample t-test against a null AUC distribution at $\alpha = 0.05$, and shown as mean±s.e.m). Note that only the network model encoded all three assays.

Figure 2: Individual electome networks within the multi-assay anxiety model independently encode distinct anxiety paradigms. A) Power and Synchrony measures that comprise each electome network. Brain regions and frequency bands ranging from 1-56 Hz are shown around the rim of the plot. Power features are depicted as bands within the rim of the plot, and cross-spectral (i.e., synchrony) measures are depicted by the lines connecting the brain regions through the center of the circle. The top 15 percent of components for each electome network is shown. **B)** Granger offset measures were used to quantify directionality for the synchrony measures shown in A. Prominent directionality features were found in multiple bands coded by color. Histograms quantify the number of lead and lagging circuit interactions for each brain region. **C)** Schematic of directionality for each of the three electome networks. Arrows are colored to represent the dominant frequency of directionally (see color scale in panels A or B). **D)** Independent predictive performance of each supervised network across each anxiety assay. Mean contribution towards the joint model logistic regression predictions is also shown. Independent predictive performance of each supervised network across each anxiety assay. Tests were performed using the 17 holdout mice, and networks that showed significant encoding are highlighted in pink (data analyzed using a one-tailed unpaired t-test against a null AUC distribution at $\alpha = 0.05$).

Figure 3: Increases in Electome Network 1 and 2 activity encodes features of anxiety related paradigms. A) Electome Network activity dynamics during fluoxetine assay. Data is plotted across 5-minute windows for Electome Network 1 (left) and 2 (right). Note that activity decreases in both networks over time following saline and fluoxetine treatment (N = 6 mice). P* <0.05 for time effect using a within and within two-way ANOVA. **B)** Comparison of Electome Network activity in safe zones of the EPM (closed arm) and BOF (periphery) over the duration of the assays. Time (P^{*}), and assay ($P^{\#}$) effects

were determined using an analysis of covariance. Data was plotted with a 10s sliding window and shown normalized to network activity observed in the home cage. **C)** Mice showed avoidance of the anxiogenic zones of the EPM (left, P<0.05 using one-tailed paired t-test) and BOF (middle, P<0.05 using one-tailed paired t-test). Bout length of mice in the anxiogenic zones for EPM and BOF (right; P<0.05 using one-tailed unpaired t-test). **D)** Decrease in Network 1 (left) and 2 (right) activity between the first and last minute of each assay. Network 2 showed a larger activity decrease in the BOF than in the EPM (P<0.05 using one-sided Mann-Whitney U test). **E-F)** Average period of occupancy in safe and anxiogenic zones in E) EPM and F) BOF assays. Note that mice showed greater occupancy of the center in the second half of the BOF. **G)** Electome Network activity dynamics relative to arm locations in the EPM assay. Gray highlights 1 second windows when the animals are in the open or closed arms. Neural activity preceding and following these timepoints is shown as well, and data is shown normalized to the mean activity observed across the assay. The purple line highlights temporal intervals with significantly different Electome Network activity, determined using a one-tailed Wilcoxon sign rank test (N = 11 mice). **H)** Same as G, except data shown for the BOF assay (N=9 mice).

Figure 4: Electome Network 1 and 2 activity does not encode arousal. A) Mice were trained to nose poke for 5 consecutive seconds. A sucrose reward was delivered at time zero, highlighted by gray. Electome Network activity was compared prior to and following sucrose delivery using a one-tailed sign-rank test (N=9 mice). Data is shown as data is shown as mean±s.e.m. **B)** Electome Network activity was quantified while mice engaged with an object or a social stimulus mouse during a free interaction assay and compared using a one-tailed sign-rank test (N=12 mice). All analyses were performed in mice that were not used to learn the multi-assay anxiety model. Data is shown as data is shown as mean±s.e.m.

Figure 5: Electome Network 1 and Network 2 activity encode distinct anxiety paradigms. A) Mice were infected with ChR2 in ventral hippocampus (Hip) and implanted with an optrode to target lateral hypothalamus (LH). Multiwire electrodes were also implanted to target the 8 brain regions utilized to learn the multi-assay anxiety network (N=11 mice). B) Neural activity recorded during optogenetic stimulation of Hip terminals in LH with blue (473nm, 20hz, 5mW, 5ms pulses) or yellow light (593.5nm, 20hz, 5mW, 5ms pulses). Note that blue light stimulation induced activity in LH (and remotely) while yellow light stimulation did not. **C)** Electome Network 1 and **D)** Network 2 activity during yellow or blue light stimulation. Network 2 showed an increase in activity with blue vs. yellow light stimulation (P<0.001 using a one-tailed Wilcoxon sign rank test)) while Network 1 did not (P=0.14). **E)** Behavioral paradigm utilized to induce fear conditioning. Conditioned mice (CS+; N=10) received an air puff at the end of each tone presentation, while non-conditioned mice (CS-; N=15) did not (top). Neural activity was recorded in both groups throughout tone presentation (bottom). **F)** Freezing behavior in CS- and CS+ mice one to two days after exposure to the conditioning paradigm. **G-H)** Mean Activity of G) Electome Network 1 and H) Electome Network 2 activity within the 10 second interval prior to the presentation of the 7^{th} conditioning tone. **I-J)** Mean activity of I) Electome Network 1 and J) Electome Network 2 within the 20 second following the presentation of the 7^{th} conditioning tone. **H-K)** Mean activity of I) Network 1 and J) Network 2 in response to an air puff. Data was analyzed using a one-tailed rank sum test.

Figure 6: Alternated Electome network activity signals behavioral disruptions in mouse models of mood disorders. A) EPM open arm exploration in WT and *ClockΔ19* mice (N=17 mice/genotype). Data was compared using a one tailed t-test. **B)** Neural activity was isolated when mice were in the closed arm of the EPM and Electome Network 1 (left) and 2 (right) activity was compared across genotype using an Analysis of Covariance (N=10 and 11 for WT and *ClockΔ19* mice, respectively; data shown as mean±s.e.m.). **C)** Distinct stress paradigms utilized to model depression in mice. **D)** Schematic of choice interaction assay utilized to quantify susceptibility to chronic social defeat stress (left), and resultant

social interaction profiles of a population of stressed mice (right). Red circles denote mice defined as susceptible (interaction ratio < 1), while green circles denote resilient mice (interaction ratio >= 1). Black circles denote non-stressed control mice. **E)** EPM open arm exploration in mice subjected to chronic social defeat stress (N=12 mice) and control mice (N=10 mice). Data was compared between stressed and non-stressed mice using a one-tailed t-test. Post-hoc testing between susceptible (N=5 mice) and resilient mice (N=7 mice) was performed using a two-tailed t-test. **F)** Electome Network 1 (left) and 2 (right) activity was quantified in the home cage and compared between chronic social defeat stressed (N=34 mice) and non-stressed controls (N=16 mice) a one-tailed rank-sum test. Post-hoc testing was compared between susceptible (N=21 mice) and resilient mice (N=13 mice) using a two-tailed rank-sum test. **G)** EPM open arm exploration in mice subjected to chronic mild unpredictable stress (N=11 mice) and control mice (N-11 mice). Data was compared using a one-tailed t-test. **H)** Electome Network 1 (left) and 2 (right) activity was quantified in the home cage and compared across groups using a one-tailed rank-sum test.

Figure 7: Conceptual framework utilized to discover and validate electome network for anxious internal state. A) Affective and neurophysiological states (listed on the left) induced by behavioral and experimental manipulations (listed along the top). Manipulations that were hypothesized to induce/strengthen the internal state listed to the left are highlighted by green. Manipulations that were hypothesized to decrease the internal state listed to the left are highlighted by red. Manipulations for which there is no clear prediction for the impact on the affect state listed to the left are highlighted by yellow. Mice used for each analysis are shown in the bottom row. New independent mice are highlighted in green. **B)** Responses of Electome Networks 1 and 2 to experimental conditions utilized throughout the study. Green and red boxes highlight conditions where network activity significantly increased or decreased, respectively. An 'X' is used to denote the non-significant trends observed in network activity response.

Methods

Animal Care & Use

Male C57BL/6J (C57) mice were purchased from Jackson Labs at 6-8 weeks of age. Unless otherwise specified, mice were housed 3-5 per cage, on a 12-hour light/dark cycle, and maintained in a humidity- and temperature-controlled room with water available *ad libitum. Clock*Δ19 mice were created by N-ethyl-N-nitrosourea mutagenesis that produced a dominant-negative CLOCK protein as previously described [38, 39]. After backcrossing >10 generations on a BALB/cJ background, *Clock*Δ19 mice and their wild type littermate controls were bred from heterozygous (*Clock*Δ19 -/+) breeding pairs. Male and female mice, 8-16 weeks old, were used for electrophysiological experiments presented in this study. *A*nxiety-related manipulations and behavioral tests were conducted with approved protocols from the Duke University Institution Animal Care and Use Committee. The elevated plus maze (EPM) behavioral experiments in ClockΔ19 mice and their littermate controls were conducted at the University of Pittsburgh. These experiments were performed in compliance with approved protocols from the University of Pittsburgh's Institution Animal Care and Use Committee. The EPM behavioral experiments in mice exposed to chronic social defeat stress were conducted at the University of Iowa. These experiments were performed in compliance with approved protocols from the University of Iowa's Institution Animal Care and Use Committee. All experiments were conducted in 6-20 weeks old mice, and in accordance with the NIH guidelines for the Care and Use of Laboratory Animals.

Data Extraction and Processing

Electrode Implantation Surgery

The electrode implantation surgery procedure has been described previously[48, 49]. Mice were anesthetized with 1.5% isoflurane, placed in a stereotaxic device and metal ground screws were secured in above anterior cranium (midline) and cerebellum (midline). A third screw was secured laterally, roughly half-way between the two other screws. Thirty-two tungsten microwires were arranged in array bundles designed to target amygdala (Amy), medial dorsal nucleus of thalamus (MD), nucleus accumbens core and shell (NAc), ventral tegmental area (VTA), medial prefrontal cortex (mPFC), dorsal hippocampus (dHip), and ventral hippocampus (Hip) and were centered based on stereotaxic coordinates measured from bregma (Amy: -1.4mm AP, 2.9 mm ML, -3.85 mm DV from dura; MD: -1.58mm AP, 0.3 mm ML, -2.88 mm DV from dura; VTA: -3.5mm AP, ±0.25 mm ML, -4.25 mm DV from dura; Hip: -3.3mm AP, 3.0mm ML, -3.75mm DV from dura; mPFC: 1.62mm AP, ±0.25mm ML, 2.25mm DV from dura; NAc: 1.3mm AP, 2.25mm ML, -4.1 mm DV from dura, implanted at an angle of 22.1°). We targeted cingulate cortex, prelimbic cortex, infralimbic cortex using the mPFC bundle by building a 0.5mm and 1.1mm DV stagger into our electrode bundle microwires. Animals were implanted bilaterally in mPFC and VTA. All other bundles were implanted in the left hemisphere (supplemental Fig. S9). The NAc bundle included a 0.6mm DV stagger such that wires were distributed across NAc core and shell. We targeted basolateral amygdala BLA and central amygdala CeA by building a 0.5mm ML stagger and 0.3mm DV stagger into our AMY electrode bundle [26]. Notably, these implantation sites have been homogenized across experimental preparations in the lab enabling comparative analysis across prior and recently collected data sets. A metal ground wire was secured to the anterior and posterior screws, and the implanted electrodes were anchored to all three screws using dental acrylic. To mitigate pain and inflammation related to the procedure, all animals except those subjected to fear conditioning, chronic mild unpredictable stress, and chronic social defeat stress received carprofen (5mg/kg, s.c.). Injections were given once prior to surgery and then every 24 hours for three days following electrode implantation.

Neural Electrophysiological Data Acquisition & Video Recording

Neurophysiological data were acquired using a Cerebus acquisition system (Blackrock Microsystems, Inc., Salt Lake City, UT). Animals were connected to the system using an M or Mu-32 channel headstage (Blackrock Microsystems, Inc., Salt Lake City, UT) and a motorized HDMI commutator (Doric Lenses, Quebec, Canada). Local field potentials (LFPs) were bandpass filtered at 0.5-250Hz and sampled/stored at 1kHz. All neurophysiological data were referenced to a ground wire connecting the ground screws above cerebellum and anterior cranium. Video recordings were acquired in real-time using NeuroMotive (Blackrock Microsystems, Inc., Salt Lake City, UT) and synchronized with neurophysiological data.

Histological Confirmation

Histological analysis of implantation sites was performed using one of two protocols at the conclusion of experiments to confirm electrode placement. Animals were perfused with 4% paraformaldehyde (PFA), and brains were harvested and stored for 24 hours in PFA. Brains were either processed on a cryostat or vibratome. For cryostat: Brains were then cryoprotected with sucrose and frozen in OCT compound prior to being stored in -80C. Brains were sliced at 35 µm using a cryostat and stained with either DAPI (AbCam) or cresyl violet (Sigma) using standard protocols. Slices were imaged at 4x and 10x magnification on a Nikon eclipse fluorescent microscope. Alternatively for brains processed via vibratome, mice were perfused with 4% paraformaldehyde (PFA, Electron Microscopy Sciences) in PBS, and brains were harvested and post-fixed in 4% PFA and then transferred to PBS with 0.05mM sodium

azide. Brains were sliced at 40um (Leica Vibrating Blade Microtome) and stained with Hoechst (Fishersci) containing mounting solution (9.6% Mowiol 4-88 (Sigma) in 24% glycerol, 0.M M Tris-Cl pH 8.5) on standard microscope slides. Slides were imaged at 4x and 10x with Olympus Slide Scanner (VS200).

LFP Processing to Remove Signal Artifact

We employed a heuristic approach to eliminate recording segments containing non-physiological signals identically to previous works [26, 50], and we paraphrase the processing procedure as follows: we first computed the signal envelope for each channel by utilizing the magnitude of the Hilbert transform. For any 1-second window in which the envelope surpasses a predetermined low threshold, we discard the entire segment if, at any point within that window, the envelope exceeds a second, higher threshold. The two thresholds were independently determined for each brain region. The high threshold was set at 5 times the median absolute deviation of the envelope value specific to that region. The choice of five median absolute deviations as the high threshold was based on its approximate equivalence to 3 standard deviations from the mean in normally distributed data, while remaining robust to outliers. The low threshold was empirically established as 3.33% of the high threshold. If more than half of the window was removed for a given channel, we also removed the remaining portion of that window for that channel. Additionally, any windows where the standard deviation of the channel is less than 0.01 were excluded.

Feature Extraction

Feature extraction was performed identically to previous works [26, 50], and we paraphrase the generation procedure as follows: LFPs were averaged across wires within the same region to generate a composite LFP measure. Signal processing was conducted using Matlab (The MathWorks, Inc., Natick, MA). For LFP Power, a sliding Fourier transform with a Hamming window was applied to the averaged LFP signal utilizing a 1-second window and a 1-second step. Frequencies ranging from 1-56Hz were analyzed. LFP cross-structural coherence was computed from pairs of averaged LFPs using magnitude-squared coherence, where coherence is a function of the power spectral densities of brain regions A and B and their cross-spectral densities.

$$C_{AB}(f) = \frac{|Psd_{AB}(f)|^2}{Psd_{AA}(f)Psd_{BB}(f)}$$

Spectral Granger causality features [51] were computed using the multivariate Granger causality (MVGC) MATLAB toolbox [52]. The data underwent a high-pass Butterworth filter with a stopband at 1Hz and a passband at 4Hz. Granger values for each window were calculated using a 20-order AR model through the GCCA_tsdata_to_smvgc function of the MVGC toolbox. Granger causality values were determined for all integer frequency values within the specified range for all directed pairs of brain regions in the dataset[50].

Acute Fluoxetine Administration (FLX)

For the behavioral fluoxetine experiments, mice were randomly assigned to receiving either an injection of fluoxetine or saline 30 minutes prior to being placed on the EPM. Fluoxetine (Sigma) was made up in 0.9% NaCl to a concentration of 1mg/mL and then injected at 10mL/kg for a final concentration of 10 mg/kg, i.p.[28]. Physiologic saline injection was injected at 10 mL/kg as well as a control for injection volume. Animals were habituated to i.p. injections daily for 1 week prior to behavioral testing. Though

fluoxetine only has an 8-hr half-life in mice, a lengthy washout period was chosen to ensure no traces of the drug remained.

For electrophysiologic recordings, animals used for training the final model followed a standard pharmacological crossover design with a 2-week washout period. Specifically, after habituation to the experimental room for 1 hour, mice were pseudorandomly assigned to receiving a or saline injection. Neural recordings were then obtained for an hour. Two weeks later, animals underwent a second one-hour recording session after receiving the other treatment. To test the final model, we utilized a protocol in which mice were two recording were performed at a much closer interval. Specifically, after habituation to the experimental room for 1 hour, mice were treated with saline and neural data was recorded for an hour. Several hours later, mice were subjected to a second recording session immediately following treatment with fluoxetine.

Elevated Plus Maze (EPM)

The EPM assay is widely employed to measure anxiety behavior in mice[53]. The EPM is comprised of four arms arranged in a cross shape, each measuring 30.5cm in length and 30.5cm in width, positioned at a height of 91.4cm from the floor. Additionally, there is a central region measuring 5cm by 5cm. Among the arms, two are designated as 'closed,' enclosed by walls that are 16.5cm in height on three sides, while the other two are 'open' and surrounded by a low piece of tape, approximately 1mm in height.

Two days prior to testing, mice were gently handled in the experimental room for roughly 1 minute per animal. Following gentle handling, mice were habituated to the testing room for 1 hour in a testing 'home cage'. After this hour, mice were returned to group housing in their original home cage. This procedure was repeated one day prior to experimental testing. On the testing day, mice were habituated to the experimental room in their individual testing home cage for one hour. Mice were then connected to the recording system and habituated for an additional 10 minutes. Following 5 minutes of neural and video recordings from an overhead camera, mice were placed in the center of the EPM facing one of the closed arms. Neural recordings and video data were acquired for an additional five-ten minutes. Testing was performed at 175lux, during the light cycle.

Bright Open Field (BOF)

The bright open field assay is also widely employed to measure anxiety behavior in mice[53]. This assay consists of a square arena (46 cm x 46 cm x 30 cm), in which the innermost third (i.e., 'center zone') is considered to be more anxiogenic zone than the outermost two thirds (i.e., 'periphery zone'). Mice were habituated to the testing room in an individual experimental home cage using the same procedure described for the EPM. On the testing day, mice connected to the recording system and five minutes of neural and video data (from an overhead camera) were acquired while mice were in their individual testing home cage. Mice were then placed in the periphery of the BOF, and an additional five minutes of data were acquired while mice freely explored the arena. Testing was performed at 125lux, during the light cycle.

Delayed sucrose reward apparatus

The task chamber was constructed from Lego Duplo pieces of varied color, shape, and size. The apparatus had approximate dimensions of 48cm wide x 35cm deep x 30cm tall, and each wall was visually distinct. A nose poke detector was in the center of each wall, placed 1cm above the floor. There

was also an LED light directly above each nose poke detector. The chamber was also equipped with four fluid dispensers, which were calibrated to release 5µL of 10% sucrose directly into each nose poke detector. The reward for three of the ports was also flavored with pumpkin, almond, or orange oil. The location and reward type remained fixed throughout each phase of experimental testing for all animals. During the task, the chamber was illuminated to 30 lux. The system was also equipped with speakers and an audiometer, and reward cues were played at 68dB. Signals from the nose poke detectors, LED lights, fluid dispensers, and audiometer were digitized and stored in parallel with our neural recordings.

Delayed sucrose reward training and task

Delayed sucrose reward task was modeled after a prior test in which mice had to remain in a spatial location in order to receive a food reward [54, 55]. After 7-14 days of recovery from surgical implantation, mice were food-deprived to 90% of their free-feeding body weight. During a training session, a mouse was connected to a recording cable, and placed in the temporal goal progress task apparatus. The training procedure is as follows:

- Stage 1: On the first day of training, mice freely accessed the testing chamber for 60 minutes. Each poke into a nose poke detector triggered a 500ms tone at 4000Hz and 5µL of reward release directly into the poke detector. This stage was repeated over 2 days.
- Stage 2: On the third and fourth day of training, mice were placed into the recording chamber together with their cage mates, without a recording cable. Mice were then allowed to freely explore the recording chamber for 120 minutes.
- Stage 3: On the fifth day, mice resumed individual training, during which they advanced in task difficulty after meeting specific criteria.
    - 3a: Each detected poke activated a 500ms 4000Hz tone and released a 5µL reward at the beginning of the tone.
    - 3b: Each detected poke activated a 500ms 4000Hz tone and released a 5µL reward at the end of the tone.
    - 3c: Each detected poke activated a 500ms 4000Hz tone and released a 5µL reward at the end of the tone if a mouse remained in the detector.
    - 3d: Each detected poke activated a 500ms 4000Hz tone and released a 5µL reward one second after the start of the tone if a mouse remained in the detector.
    - 3e: Each detected poke activated a 500ms 4000+387Hz tone, and a second 500ms 4000Hz tone, one second later. A 5µL reward was released at the end of 1.5 seconds if a mouse remained in the detector.
    - 3f: Each detected poke activated a 500ms 4000+387Hz tone, and a second 500ms 4000Hz tone, one second later. A 5µL reward was released at the end of 2 seconds if a mouse remained in the detector.
    - 3g: Each detected poke activated a 500ms 4000+387+387Hz tone, and a second 500ms 4000+378Hz tone one second later, and a final 500ms 4000Hz tone one second later. A 5µL reward was released at the end of 2.5 seconds if a mouse remained in the detector. This training pattern continued until mice passed training at the 5-second delay. For these trials, a tone of diminishing frequency was played at the beginning of each second, and mice received reward if the poke hole was activated for the entire test interval.
- A mouse passed a training stage when it completed 120 rewarded pokes in one day, or 120 rewarded pokes in two consecutive days and the second day reward count was greater than or equal to the reward count of the first day. Mice regressed to a prior training stage if they failed

to complete a stage after five days, or if they received fewer than twenty rewards during a session. The data utilized for our electrophysiological analysis was acquired after mice completed training at the 5-second delay.

Social Preference Assay

A previously published data set was used to assess the impact of social interaction on electome network activity [26]. Briefly, mice implanted with electrodes at the same brain coordinates utilized for this study were allowed to explore a rectangular arena (61cm × 42.5cm × 22cm, L×W×H) for 10 minutes. Two clear plexiglass walls divided the area into two equal chambers. Each chamber contained a circular holding cage (8.3cm diameter and 12cm tall) containing either a novel object or a C3H target mouse matched for sex and age. Data was collected across 6-10 testing session/mouse. Video data was tracked using Bonsai Visual Reactive Programming software, and network activity was analyzed for periods in which mice were within ~5cm of the novel object or target mouse.

Optogenetic Stimulation and Electrical Recordings

We modeled previously published methods for targeting the ventral hippocampus → lateral hypothalamus circuit [20]. Specifically, mice were anesthetized with 1.5% isoflurane, and placed in a stereotaxic device. A 33-gauge Hamilton syringe was used to bilaterally infuse 0.5 µl of AAV5-ChR2-EYFP at a rate of 0.1 µl/min into ventral hippocampus (-3.16mm AP, 3.3mm ML, -3.75mm DV from dura). Two weeks, later mice were implanted with recording electrodes using the procedure and brain targets described above ('Electrode Implantation Surgery'). These electrodes included a bundle that was used to target lateral hypothalamus (LH: −1.95AP, 0.5ML, −4.75DV). A 100µm diameter fiberoptic (Doric Lenses) fiberoptic cannula was built into the LH bundle with the tip situated 250µm above the tip of the LH microwires bundle [56, 57]. *In vivo* recordings were conducted after 2 weeks of recovery. Mice were habituated to the experimental room/setup for the two days preceding experiments.

Mice were connected to the recording system using a 32-channel M headstage, and a fiberoptic patch cable, and placed in a new home cage for 1 hour. On the testing day, mice were connected and placed in the same experimental home cage. After 40 minutes of additional habituation, neural data was recorded for 20 minutes. Mice were then stimulated with blue or yellow light for 10 minutes. Light stimulation was delivered at 20hz, 5mW, with 5ms pulses and verified using a power meter (Thorlabs, PM100D). Mice were pseudorandomized to stimulation with either blue (473nm wavelength, CrystaLaser, CL473-025-O) or yellow light (593.5nm, OEM Laser Systems, Model No. MGL-F-593.5/80mW).

One week later, mice were subjected to a second recording with the other laser, using the same protocol described above. Thus, each mouse was stimulated with blue and yellow in pseudorandomized order across the two sessions.

Fear Conditioning

Mice were implanted with electrodes as described above ('Electrode Implantation Surgery'). Following a two-week recovery period, mice were trained in a classic cued fear conditioning paradigm during which an auditory tone (conditioned stimulus; CS) was paired with an aversive air puff (unconditioned stimulus, US). The CS consisted of a 30 second, 10 kHz, 80dB, continuous auditory tone that was generated using MATLAB. The US consisted of a 2-second, 40 PSI, air-puff that was introduced through 4 pumps built into each of the testing chamber's walls. Mice were randomly assigned to 2 groups: Fear conditioned (CS+/US+) and Control (CS+/US-). Behavioral testing was conducted in two distinctly different behavioral

contexts (context A and B). Context A was a 10”×10”×11” (L×W×H), striped chamber made of alternating black and white Legos®. Context B was 6”×12×11” chamber, with walls consisting of mixed colored Legos. Context A had a smooth floor, while context B had a textured floor.

Prior to conditioning (Day 0), mice were habituated to the behavioral room for 2 hours. On Day 1 of the task, mice were connected to the recording system, and placed into context A for 2 minutes. The conditioned group was exposed to 7 trials of the CS. The US was presented during the last 2 seconds of each tone, and there was a pseudorandom interval ranging from 60-120 seconds between each trial. The control group was exposed to 7 trials of the CS without the US. Each group remained in Context A for 1 minute after the last trial concluded. The neural and video data were collected throughout the recordings. We also collected a continuous signal corresponding to the onset and offset of the CS.

Mice were then exposed to a cued recall session on Day 3. Here, mice were connected to the recording system and placed into Context B. After 3 minutes, mice were presented with the CS for 3 minutes. Neural and video data was recorded throughout this interval, and the freezing behavior was quantified using Ethovision X12 (Noldus, Wageningen, the Netherlands) to detect the percentage of time during the CS presentation that the animal did not move. A subset of the conditioned mice (N=5) was also exposed to an extinction protocol on Day 2. For these experiments, mice were presented with the CS, but not the US, in Context A. Since our objective was to quantify neural responses to fear conditioning on Day 1, and exposure to the one-day extinction protocol had no impact on freezing behavior on Day 3 (t_{26}=0.11 and P=0.92 using two-tailed unpaired t-test), we pooled all the mice in the CS+/US+ group for the analyses presented in the text.

Chronic Social Defeat Stress (cSDS)

These methods parallel those described in our prior work [27, 57]. Data for our electrophysiological and behavioral analyses were obtained from two different cohorts of implanted mice. Behavioral data on the EPM was assessed from mice implanted in a different set of brain regions than those used for this study. Neurophysiological recordings in the home cage were obtained from mice implanted in the same brain regions utilized in this study. Data from a subset of these mice were presented in our published work [26].

We modeled our chronic social defeat stress protocol after previously published work [42, 46]. Singly housed male retired-breeder CD1 (Charles River) mice were used as resident aggressors for the social defeat. Experimental animals were pseudorandomly assigned to control or stress groups, such that cage mates were distributed across groups. Six to seven-week old male mice were implanted with electrodes as described above (‘Electrode Implantation Surgery’). Stress experiments were initiated two weeks after surgical recovery. All C57Bl6/J (C57) mice were singly housed prior to being subjected to cSDS, and highly aggressive CD1s were used for the stress protocol. Briefly, C57 experimental mice were exposed to CD1 aggressors for 5 mins and only removed early in the event of serious physical injury (which never happened for more than two defeated mice animals per defeat). Defeats were run in dim light conditions (~40-50 Lux). After 5 mins, C57 mice and CD1 aggressors were separated with a perforated divider for 24 hours. Control C57 mice were placed on either side of a similar cage setup and cage-mates were rotated each day. This process was repeated for a total of 10 days. Triage was performed on animals following each day of defeat to check for and treat any wounds. After this check, the lights were turned off., Mice that exhibited significant injuries during social defeat stress were removed from post-stress analysis.

All control and stressed mice were subjected to neural recording in their home cage one day following completion of the chronic social defeat stress protocol. Mice were then subjected to a forced interaction test during which they were placed in a semi-protected circular sub-chamber. After ten minutes, a novel CD1 aggressor mouse was placed within the same arena directed outside sub-chamber for 5 minutes [27, 57, 58].

A choice social interaction test was used to categorize stressed mice as susceptible or resilient [41, 42, 57, 58]. This assay was performed 2 days following the last social defeat session, during the dark cycle of each mouse. Testing was conducted in a room with two red lamps facing the ceiling (2-10 lux). Animals were habituated to the room for approximately two hours prior to the start of testing. Experiments were randomized and balanced to include alternating control and experimental mice spread throughout the duration of experiment. For each trial, an animal was placed in the center of an opaque, white, 18” x 18” box with 18” high walls with a wire-mesh sub-chamber at the center of one wall for 150 seconds. Then a CD1 mouse (low/non-aggressive) was placed in the enclosed sub-chamber, and the experimental mouse was placed back in the box for 2 minutes and 30 seconds. Behavior was recorded for the entirety of each trial. Stressed mice that showed higher interaction time with the empty sub-chamber than the sub-chamber containing the CD1 mouse were defined as susceptible. Mice that showed higher interaction time with the sub-chamber containing the CD1 were defined as resilient. Between mice, all chambers were cleaned with Super Sani-Cloth germicidal disposable wipes (PDI, Orangeburg, NY) or 70% ethanol, and dried with kimwipes. Data was analyzed using Noldus Ethovision version 15.

Mice subjected to cSDS and their non-stressed controls were tested in the EPM 12 days following the last social defeat session. Animals were tested during their dark cycle in a dark room with two red light lamps facing the ceiling (2-10 lux at the surface of the behavioral arena). Animals were acclimated to the room for >1 hour prior to starting experiments during their dark cycle. For each experimental trial, animals were placed in the center of the apparatus facing the same side each trial and allowed to explore the maze for 5 minutes. After 5 minutes, the animal was removed from the apparatus and placed back into its home cage. The trials were randomized and balanced with alternation of control and experimental animals. After each run, the EPM was thoroughly cleaned with Super Sani-Cloth germicidal disposable wipes (PDI, Orangeburg, NY) and dried with kimwipes. Data was analyzed using Noldus Ethovision version 15.

Chronic Mild Unpredictable Stress

We modeled our chronic mild unpredictable stress protocol after previously published work [44, 45]. C57 male mice were implanted with electrodes to target the same brain regions utilized to learn the anxiety related networks, at age 7-9 weeks. Two weeks later, cages of mice were pseudorandomized into a stress or control group. Control mice were subjected to gentle handling twice a week. The stress group was exposed to 2 aversive experiences each day – one during the light cycle and one during the dark cycle – for eight weeks, as previously described [44]. The stressors were as follows:

- physical restraint – mice were placed in a ~50mL plastic cone (with openings for breathing on both ends) for 1 hr
- shaking – a cage of mice was placed on an orbital shaker for 1hr at 60 rpm
- overnight illumination – mice were exposed to regular room light during the 12 hr dark cycle
- inverted light cycle – mice were exposed to dark-cycle room conditions during the light cycle and light conditions during the dark cycle
- tilted cage – cages were tilted at a 45 degree angle for 12 hrs

- strobe – mice were placed in a room with a strobe light during the dark cycle for 12 hrs
- wet bedding – cage bedding was saturated with water for 12 hr
- soiled rat bedding – cage bedding was replaced with used rat cage bedding for 3 hrs
- cold exposure – mice were placed in a cold room (4°C) for 1 hr
- missing bedding –bedding was completely removed from the cage for 12 hr.
- food and water restriction – food and water was removed for 12 hr during the dark cycle
- overcrowding – cage space was reduced by 50% for 12 hr during the dark cycle

Stressors were presented in pseudorandomized order. Body weight was monitored once a week to ensure mice didn't lose more than 10% body weight during the stress proposal.

Model Selection and Training

Label Assignment for Training Datasets

To make use of supervised machine learning methods, per-sample anxiety state labels must be assigned for our training assays. For the acute FLX assay, we accounted for drug activation time and assigned all timepoints within the last 30 minutes of the 1-hour recording to either a heightened or lower anxiety state after mice received FLX or saline, respectively. For the EPM and BOF assays, anxiety states within the assay can be ambiguous. To prevent mislabeling of anxiety states in assays, we assign all timepoints for which mice are in the EPM or BOF as a heightened anxiety state. We then make use of recordings taken while the mice are in their home cage environment and label those as a lower anxiety state. With this formulation, all three training assays now have the same labeling nomenclature of heightened anxiety and lower anxiety states regardless of the anxiogenic assay, allowing for easy combination and comparison during model training.

Training, Validation, and Test Splits

Once features had been extracted for the FLX, EPM, and BOF assays, mice were subsequently split into three groups: training data, validation data, test data. These splits were performed by mouse such that all data belonging to a mouse was all contained in the same group. Splitting by mouse is critical as it prevents a machine learning model from simply learning the identity of a mouse in the training data to achieve inflated performance on holdout data. Additionally, we wished to see how our model performs on data from completely new subjects, which is a situation analogous to the conditions of a clinical setting. Training data and validation data were used for model development where many sets of hyperparameters and model formulation may be tested. Test data were kept as true hold out data, which we did not observe or test our model on until the final model architecture was determined. Several mice were placed in more than one assay; therefore, care was taken to ensure that all such mice were in the same group across all assay splits. That is, if a mouse was in the training group for the FLX assay, then it should be in the training group for all other assays. Once final model parameters were determined, training and validation datasets were combined for a final training run, which was then validated on the test data. Training, Validation and Test groups had: 9, 4, and 6 mice respectively for the FLX assay; 21, 5, and 11 mice respectively for the EPM assay; and 16, 3, and 9 mice respectively for the BOF assay. There were 17 mice from the training groups, and 7 from the test groups were shared in 2 assays (only between EPM and BOF). There was a single mouse in the test group that was exposed to all three assays.

Discriminative Cross-Spectral Factor Analysis (dCSFA-NMF)

Discriminative Cross-Spectral Factor Analysis - Nonnegative Matrix Factorization (dCSFA-NMF) is a machine learning framework for discovering key predictive factors relevant to a behavioral assay or emotional state of interest [25]. This method has been used previously to detect brain networks corresponding to stress and social activity in mice using LFP data[26]. Similar to other factor models that have been used in neuroscience, such as PCA, ICA and NMF, dCSFA-NMF identifies underlying components, interpreted to be networks, of connectivity. The superposition of these networks then explains the observed neural activity. While the previously mentioned unsupervised methods can identify networks of activity, discovered networks are learned to explain the maximum amount of the observed neural activity. As it is unlikely that anxiety and other emotional states make up one of these dominant networks, dCSFA-NMF makes use of a supervision component to ensure that one or more of the networks are correlated with a behavior or emotional state of interest.

Rigorously, the model learns K fixed components $W \in \mathbb{R}^{K \times M}$ that can reconstruct observed data $X \in \mathbb{R}^{N \times M}$ using an array of network activity scores $s \in \mathbb{R}^{N \times K}$ such that $X = sW$. W and s are also constrained to be positive as the features of use – power, coherence, and Granger causality – observed in X are also non-negative. Network activity scores are inferred from the observed data using an encoder function $s = f_\theta(X)$, which can take the form of a neural network or linear model. The activity scores $s_s \in \mathbb{R}^{N \times Q}$ of the $K \geq Q \geq 1$ supervised components are then used in a logistic regression model f_ϕ to predict the behavior of interest $y = f_\phi(s_s)$. We constrain our predictions to use a sparse combination of all networks, namely only the supervised networks, to narrow the scope of our network discovery and reduce the total number of comparisons. The parameters of the model are then optimized using the loss function,

$$\min_{W,\theta,\phi} \sum_{i=1}^{N} \mathcal{L}_x\big(x_i, W f_\theta(x_i)\big) + \lambda \mathcal{L}_y\Big(y_i, f_\phi\big(f_\theta(x_i)\big)\Big) + \alpha \mathcal{L}_{w_s}\big(x_i, W f_\theta(x_i)\big).$$

Here, $\mathcal{L}_x$ is the reconstruction error between the original power, coherence, and Granger features and those generated by the product of our network scores and networks, sW. In this work we make use of the Mean-Squared-Error (MSE) function. Our predictive loss $\mathcal{L}_y$ is a binary cross-entropy loss and penalizes our model for incorrectly predicting the behavioral state of each window. The impact of the predictive loss can be tuned using the hyperparameter λ. Lastly, we impose a second reconstruction loss, $\mathcal{L}_{w_s}$, on the supervised network scores. This reconstruction loss prevents our neural network encoder f_θ from learning an uninterpretable near-zero noise embedding for the supervised scores that predicts well with little to no contribution to explaining neural activity. This loss can be formulated as another MSE loss between the outer product of the supervised network activations and the supervised electome network and the features. Alternatively, this loss can be formulated as a penalty to drive the supervised network scores to reconstruct the residual of the unsupervised networks and features. We used the latter in our analysis.

Performance Metrics – Predictive Modeling

To evaluate the predictive performance of our model, we used the receiver operating characteristic curve area under the curve (ROC-AUC). This metric is common in machine learning literature and can be viewed as a class rebalanced accuracy. AUC takes values on the range [0,1] where AUC=0.5 indicates chance performance in prediction. AUC=1 indicates that the model is perfectly predicting class

assignment, and an AUC=0 indicates that the model is perfectly predicting but with a flipped labeling. AUC can also be evaluated using the Mann-Whitney-U statistical test.

For evaluating our models, we obtained an AUC for each mouse and then reported the group mean and standard error of the mean for each paradigm. Many of our behavioral contexts have varying recording lengths and by reporting AUC for each mouse separately, we addressed the possibility of our model overfitting to the neural activity of mice in paradigms with longer recordings and therefore more samples. Furthermore, emotional states such as anxiety are complex and often have heterogenous presentations across individuals. By reporting AUC by mouse, we opened opportunities for post-hoc analyses into mice with heterogenous predictions. In short, by evaluating AUC by mouse, we allowed for more uniform evaluation across a wide variety of anxiogenic contexts, a cleaner evaluation of model generalizability, and post-hoc data analysis.

Performance Metrics – Generative Modeling

We take interest in how well our models explain neural activity in the brain. We evaluated how well this is done by quantifying the mean-squared-error of the model's predicted power, coherence, and Granger causality features and the originally observed values.

$$MSE(x, \hat{x}) = \frac{1}{N}\sum_{n=1}^{N}(x_n - \hat{x}_n)^2$$

During model training, we weighted the reconstruction of each of our feature types (power, coherence, Granger) by their prevalence, such that power holds equal importance to coherence and Granger despite representing a smaller number of power features.

Performance Metrics – Model Consistency

To evaluate representation consistency in our model, we used the cosine distance formula which calculates the angular distance between two vectors on a scale of $[0,1]$ due to the positivity constraint of the vectors, where 0 represents perfect alignment and 1 are completely orthogonal vectors. The cosine distance between two vectors, A and B is given by:

$$\mathcal{D}(A, B) = 1 - \frac{A \cdot B}{\|A\|\|B\|}$$

We then calculate the cosine distance between each supervised network in each fold and all supervised networks in all other folds. Using the Hungarian Matching Algorithm [59], we then pair each supervised network in each fold with the best supervised network in each other fold such that each network has a unique match in each fold. We then weighted the cosine distance between matched networks by the impact that a network score had on the prediction relative to the other networks in the same fold, such that predictive networks had a higher weighting than non-predictive networks. We performed this weighting scheme to reduce penalization of mismatched networks that were not used to predict behavior, and were thus likely irrelevant to the underlying dynamics of anxiety. This metric captured the distance between the most similar networks across runs. A consistent representation or network discovery will yield a low distance score.

Hyperparameter Selection Strategy

The dCSFA-NMF model requires selection of several hyperparameters. These factors include the number of electome factors K, number of supervised networks Q, the importance of the supervised task λ, and the importance of the supervised factor reconstruction α. Generally, the number of electome factors control how well we can reconstruct the original LFP data. The number of supervised networks does not greatly affect the overall prediction quality (Supplemental Fig. S3), however, increasing the total number of supervised networks can significantly improve the representational consistency of the behaviorally relevant networks discovered. This improved consistency is critical for validation of our networks and for using network representations to motivate future hypotheses and experiments. Identifying a suitable number of supervised networks is especially crucial in the case where multiple true underlying networks may be driving the emotional or behavioral state. Underspecifying the number of supervised networks to learn may result in the model inconsistently swapping across a subset of these suitable underlying networks.

To choose the value of K, we performed grid-search cross validation using $K = \{2,4, \dots ,58\}$. Each model was trained on the training mice for all three assays jointly and evaluated on the validation mice for all assays, per the multi-assay training procedure. We observed that the predictive performance of all three assays stabilized at K=18 with little change across all three assays for subsequent values. Subsequently, we found that the reconstruction performance plateaued at K=30. Given that the predictive performance was consistent for K>18, we selected K=30 as the total number of networks that our model would learn.

To choose a value of Q, we aimed to balance 3 design priorities in our model formation. First, our model must be predictive of the behavior of interest. Second, our model should find a relatively consistent solution (i.e. discovered brain networks should be similar across multiple runs). Lastly, our solution should be simple. Suppose we were to supervise all the networks in our model. We likely would achieve strong predictive performance; however, multiple-hypothesis testing problems would arise as we begin to test the relationships of each network with behavior. Therefore, we wished to find a stable, predictive solution that makes use of the smallest Q number of supervised networks possible. To ascertain the value of Q we should use, we tested our model with values $Q = \{1,2,3,4,5,10,20\}$ with $K = 30$.

To evaluate predictive performance of our model, we performed 4-fold cross-validation-over-subjects for each value $Q \in \{1,2,3,4,5,10,20\}$ and evaluated predictive performance on each fold's validation data. We observed that the average AUC across all three assays peaks around $Q \in \{3,4\}$ and declined slightly as the number of supervised networks greatly increased.

Additionally, we constrained our model to only identify supervised networks with scores that positively correlated with predicting a heightened anxiety state, as we aimed to discover an anxiety network rather than an anxiety inhibition network.

We selected stochastic gradient descent as our optimization algorithm as SGD is known to offer better generalization performance despite requiring longer training times [60]. We used a learning rate of .001 and a momentum value of .9.

We found that pretraining our model factors provided a substantial improvement on representational stability and predictive accuracy. We performed pretraining on our factors by training a traditional non-negative matrix factorization model on our data, and then sorting the components based on their correlation with network performance. For our multi-assay training formulation, our datasets were imbalanced with the longer-duration FLX recordings making up a much higher percentage of our total data, so we bootstraped samples in EPM and BOF such that each experimental context is equally

influential on our network pretraining. We then froze the weights of our sorted NMF factors and trained the encoder to learn scores corresponding to the fixed factors and the classifier to predict corresponding labels based on those scores. We found that training the encoder and classifier for 500 epochs was sufficient for the optimization algorithm to converge and stabilize at a minimum of the loss function. After pretraining, we then unfroze all parameters and trained them jointly. We found that an additional 500 epochs were sufficient for the model training to converge and stabilize at a minimum of the loss function.

Single-assay Model Formulation and Training

For single-assay model training, we isolated one of our three training assays (EPM, BOF, FLX) to use as our training dataset for dCSFA-NMF. While we focused on our model training using the FLX assay in the results section, we also trained models using the EPM and the BOF as singular training datasets. Each of our three single-assay models used the same labeling structure outlined above, where for the EPM data, home-cage windows were labeled as a low anxiety state and EPM windows are labeled as high anxiety state. For the BOF assay, home cage windows were labeled as a low anxiety state and BOF windows were labeled as a high anxiety state. Lastly, FLX assigned saline windows as a low anxiety state and fluoxetine windows as a high anxiety state.

Models were trained using 4-fold cross validation, where fold training and validation splits were made by partitioning the non-holdout mice into 4 separate permutation groups of training and validation mice. Predictive performance was evaluated on the concatenated training and validation partitions of the other two assays not used for model training. It is worth noting that some bias exists in this evaluation, as some mice in the other two assays may be present in the training set of the training assay. However, even with this bias, these models failed to generalize across assay. The test, or holdout, partitions of all three assays are left untouched as each of the single-assay models failed to generalize to the validation sets of all three assays jointly.

We ultimately performed our single-assay model analysis twice. First, we trained the models using a single supervised network and a comparable procedure to prior similar works[26]. Second, after we identified the value of multi-assay training and tuning for multiple consistent predictive networks, we reperformed our single training analysis with three supervised networks and 27 unsupervised networks to allow for one-to-one comparison to the multiple-assay model. This second round of training was important as we wished to properly attribute whether generalization improvements came from increased predictive capacity or were due to the multiple assay training procedure. While only the results using three supervised networks are shown throughout the text, the same trends (i.e., failure to generalize) were observed for our models using one supervised network.

Multiple Assay Model Formulation and Training

As mentioned above, our multiple assay model formulation involves concatenating the EPM, FLX, and BOF training datasets into a single training dataset. As the labels of each of these assays are distilled into heightened anxiety and lower anxiety states depending on the assay of interest, simple concatenation is possible.

For multiple assay model training, we first perform 4-fold cross validation on the training and validation partitions of all three assays for hyperparameter tuning. Like our training partitions discussed in the Train, Validation, Test splits section, we constrain our fold partitions such that if a mouse is in the

validation split for one assay, it cannot be in the training split for another assay and vice versa. This is necessary to remove bias in our evaluation.

Finally, training and validation partitions for all three assays are concatenated into a final training dataset. We then train our model using the final set of hyperparameters discovered in our hyperparameter tuning section and evaluate the model on the holdout test sets for each of the three assays.

Model Validation

Networks Decoded Assays Jointly

Given that our dCSFA-NMF model was trained to learn three separate networks, we wished to validate that each of the learned networks are not simply learning to predict for each of the three training assays independently. Networks that truly captured anxiety should not be relevant to only one context where anxiety may be experienced, but should generalize to multiple contexts. Here, we evaluated the per-mouse AUC of each of the networks separately using the Mann-Whitney-U test for each of the three training assays (Fig. 2D).

Individual Network Contribution Towards Prediction

We also consider the possibility that one or more of our networks may not contribute substantially to the overall prediction of the mouse internal state. To evaluate this, we considered the mean prediction logit of each network given by the mean network score multiplied by its corresponding logistic regression coefficient and normalized it by the sum the mean prediction logits of all supervised networks. More formally, we define the mean logit of an individual network as $z_j = \bar{s}_j \phi_j$, where $\bar{s}_j$ is the mean network activity score from the holdout data for network j and ϕ_j is the dCSFA logistic regression coefficient corresponding to that network activity score. Since we constrained our network to have positive network activity scores and logistic regression coefficients, no absolute value or squaring of the logits is necessary for comparison. We then evaluate the contribution of each network j as:

$$Contribution(j) = \frac{z_j}{\sum_{i=1}^{K} z_i}$$

This metric quantifies the average predictive impact of each network on the holdout data.

Detailed Methods for validation analyses

Location-based dynamics in network activity

To compare post-exposure effects for the safe and unsafe zones in the EPM/BOF on Network 1 and Network 2 dynamics, we extracted data from each timepoint in each location. We also extracted data in the five seconds preceding and following these timepoints. Here, the locations of C57 mice (closed arm/open arm/center for EPM and center/periphery for BOF) were encoded using Ethovision on 50 frame-per-second video recordings of the task, tracked at 25fps based on their center of mass. Frame labels were then aligned with our one-second resolution LFP features by assigning the label of each window to be the label making up most of the Ethovision frames for that timepoint. For The *ClockΔ19* mice and their littermate controls, the location was determined based on their head location. A window was labeled as open arm if 20% of the Ethovision frames corresponded with the open arm location.

We then determined the Network 1 and 2 activities at all timepoints where the mouse is in the region of interest and the network activity for all observed timepoints within a +/- 5 second window from the central timepoint. Timepoints for which electrophysiology, and therefore network scores, are not observed due to electrophysiological artifact, were dropped. For each mouse, network activity was averaged within the -5 to -1s window, the 1s to 5s window, and the instantaneous location window. Activity was then compared between locations across mice.

We then determine the Network 1 and 2 activities at all timepoints where the mouse is in the region of interest and the network activity for all observed timepoints within a +/- 5 second window from the central timepoint. Timepoints for which electrophysiology, and therefore network scores, are not observed due to electrophysiological artifact, are dropped. For each mouse, network activity was averaged within the -5 to -1s window, the 1s to 5s window, and the instantaneous location window. Activity was then compared between locations across mice.

Fluoxetine Network Dynamics

We validated our network's ability to decode anxiety attenuation post-injection with saline or fluoxetine in the holdout mice from the FLX training task. Mice were injected with saline or fluoxetine at t=0 and we recorded neural activity for one hour post-injection. We then observed Network 1 and 2 activity during the full hour recording for the 6 holdout mice. Network activity scores were binned and averaged at a 5-minute resolution with the mean and standard error activity across mouse plotted in Fig. 3B. It is worth restating that our model was trained only using timepoints during the second half of the one hour-long recorded data. While our model was biased to distinguish between fluoxetine and saline due to our model training task, the model had no prior exposure to timepoints between t= [0,30] and no explicitly supervised trend for those timepoints. Time effects were analyzed using a two-way repeated measured ANOVA.

Delayed sucrose reward task

We examined Network 1 and 2 activity during the delayed sucrose reward assay to validate that our networks are not encoding reward or arousal. Pump events for delivering sucrose to the mice were much shorter than our one-second windows, therefore we used the event-triggered feature extraction code. We collected LFP features for 4 seconds prior and 4 seconds post the pump event. These features were then projected into Networks 1 and 2. Mean network activity at one second prior and one-second post-pump event were then compared across mice (n=8) using a one-tailed Wilcoxon sign rank test.

Optogenetic Stimulation of Ventral Hippocampus to Lateral Hypothalamus circuit

We quantified network activity during optogenetic stimulation of the ventral hippocampus to lateral hypothalamus circuit. We have previously demonstrated that in the absence of ChR2, blue light stimulation has no direct impact on LFP activity using our recording approach[56]. Moreover, yellow light stimulation has no direct impact on LFP activity in the presence of ChR2[26, 49]. Thus, we chose to compare network activity during yellow light stimulation and blue light stimulation. This approach enabled us to perform within-subject comparisons.

Fear Conditioning

For Network 1 and Network 2 validations, event-centered features were extracted for 10 seconds prior to the tone and 20 seconds after the tone. Mean Network 1 and 2 scores were then calculated for the

control and conditioned mice for both the 10 seconds pre-segment and the 20 seconds post-segment separately. For both intervals, we performed one-tailed Wilcoxon rank sum tests to compare across control and conditioned mice during the 7th and final tone/air puff event. We isolated the 7th event under the assumption that the conditioned mice have successfully paired the tone stimulus with the air puff stimulus because of the 6 prior trials.

Statistical Analysis Philosophy

We trained a multi-region multi-assay model to putatively encode the anxiety state. We focused our subsequent analysis on Electome Network 1 and 2 since these networks independently encoded all three of our initial anxiety assays, and they showed the highest contribution to the joint predictive model. We then trained models to test whether this putative state was encoded by single regions and/or by pairs of brain regions. We assessed each model independently for the three assays. Based on our prior observations that other emotional internal states could not be decoded from individual brain regions [26, 27, 50], we hypothesized that activity from single regions and/or pairs of regions would fail to decode a convergent anxiety state as well. To increase the likelihood of falsifying our hypothesis we chose to leave all our statistical analysis using single region/pairs of regions uncorrected. We observed that $P>0.05$ for at least one assay for each single region/pairs of regions test. Since correcting for multiple comparisons would have served to further increase the P-values, we concluded that no single region/pairs of regions encoded a convergent anxiety state.

Next, to validate the multi-region multi-assay networks, we recorded LFP data in the same brain regions from new mice and/or new paradigms and subsequently projected these data into these two networks. We tested each network independently to elucidate their individual dynamics relevant to anxiety and their contextual limitations. Validation of Networks 1 and 2 involved various statistical tests and procedures. For comparison of anxiogenic vs. non-anxiogenic conditions, we performed non-parametric statistical tests on mean network scores for intervals or groups of interest. In cases where parametric tests are useful, such as examining network dynamics over time, we performed a Box–Cox transformation of the network activity scores prior to statistical testing. In many of the validation tests, we expected the activity of Network 1 and/or Network 2 to be higher than the control condition as we expected or behaviorally validated that anxiety levels are elevated. For these cases, we performed statistical tests with a one-tailed test. A similar approach was implemented for our control experiments using sucrose and social reward, as well. We hypothesized that anxiety-related behavior and network activity would be lower in a mouse model of mania, thus we performed one-tailed statistical tests when appropriate. All such cases are disclosed in our results section. All p-values are reported as uncorrected p-values across both networks.

In some cases, such as examining network dynamics in the safe regions over time (Fig. 3B), missing observations cannot be determined to be missing completely at random. Therefore, in such cases, we make use of an ANCOVA analysis strategy, which is flexible with missing data and allows analysis of dynamics over time. A disadvantage of this approach is that samples are treated independently without concern of group identity.

Visualization

Networks were visualized as chord plots using code adapted from https://github.com/carlson-lab/lpne/ to allow for recoloring of frequency bands. Significant features were determined by calculating the average percent contribution of each network towards the reconstruction of each feature for the training

task holdout mice. This strategy results in an even appraisal of low and high frequency features, even though low frequency spectral features tend to have higher magnitude. We then plotted the 85th percentile of these contributions, which is a threshold that adequately highlights dominant features without cluttering the plot and is consistent with related works [26].

Reproducibility

Computational Environment and Codebase Disclosure

Preprocessing and feature extraction code was performed in MATLAB R2022a using the LFP feature extraction pipeline found on the main branch at https://github.com/carlson-lab/lpne-data-analysis. Event-triggered feature extraction code can be found on the "framewindows" branch of the same repository. A PyTorch implementation of dCSFA-NMF can be found at https://github.com/carlson-lab/lpne/. All code for network generation, hyperparameter tuning, model implementation, plotting, and a singularity definition file for replicating our Python environment can be found https://github.com/carlson-lab/Anxiety. Development was performed on a computer cluster in a Singularity Container managed Python environment with nodes utilizing an NVIDIA RTX 2080 Ti.

Author Contributions – Conceptualization DNH, MHK, RCH, SDM, DEC and KD; Methodology, DNH, MHK, WEC, DEC, and KD; Formal Analysis, DNH, MHK, KKWC, GET, YG, YF, MT, and KD; Investigation, DNH, MHK, KKWC, GET, YG, DW, AM, YF, MT, AF, NMG, and KD; Resources, CAM, RCH, DEC and KD; Writing – Original Draft, DNH, MHK, JMZ, DEC, and KD; Writing – Review & Editing, DNH, MHK, KKWC, CAM, JMZ, RH, SDM, DEC, and KD; Visualization, DNH, MHK, DEC, and KD; Supervision, CAM, RCH, DEC and KD; Project Administration, DEC and KD; and Funding Acquisition, DNH, RCH, DEC, and KD; (see Supplemental Table S1 for experiment specific contributions).

Declaration of Interests

The authors have no competing financial interests.

Acknowledgements

We would like to thank Elise Adamson, Jake Benton, and Rachel Fisher-Foye for technical assistance, and Karim Abdelaal for comments. This work was supported by Hope for Depression Research Foundation, and NIH Grants 1R01MH099192 and R01MH120158 to KD. A special thanks to Freeman Hrabowski, Robert and Jane Meyerhoff, and the Meyerhoff Scholarship Program.

References

1. Szuhany, K.L. and N.M. Simon, *Anxiety Disorders: A Review.* JAMA, 2022. **328**(24): p. 2431-2445.
2. Ruscio, A.M., et al., *Cross-sectional Comparison of the Epidemiology of DSM-5 Generalized Anxiety Disorder Across the Globe.* JAMA Psychiatry, 2017. **74**(5): p. 465-475.
3. Czeisler, M.E., et al., *Mental Health, Substance Use, and Suicidal Ideation During the COVID-19 Pandemic - United States, June 24-30, 2020.* MMWR Morb Mortal Wkly Rep, 2020. **69**(32): p. 1049-1057.

4. Taylor, J.M. and P.J. Whalen, *Neuroimaging and Anxiety: the Neural Substrates of Pathological and Non-pathological Anxiety.* Curr Psychiatry Rep, 2015. **17**(6): p. 49.
5. Robinson, O.J., et al., *The translational neural circuitry of anxiety.* J Neurol Neurosurg Psychiatry, 2019. **90**(12): p. 1353-1360.
6. Takagi, Y., et al., *A common brain network among state, trait, and pathological anxiety from whole-brain functional connectivity.* Neuroimage, 2018. **172**: p. 506-516.
7. Lai, C.H., *Task MRI-Based Functional Brain Network of Anxiety.* Adv Exp Med Biol, 2020. **1191**: p. 3-20.
8. Kirkby, L., et al., *An amygdala-hippocampus subnetwork that encodes variations in human mood.* Cell, 2018. **In press**.
9. Moreira, C.M., et al., *Exploratory behaviour of rats in the elevated plus-maze is differentially sensitive to inactivation of the basolateral and central amygdaloid nuclei.* Brain Res Bull, 2007. **71**(5): p. 466-74.
10. Ciocchi, S., et al., *Encoding of conditioned fear in central amygdala inhibitory circuits.* Nature, 2010. **468**(7321): p. 277-82.
11. Calhoon, G.G. and K.M. Tye, *Resolving the neural circuits of anxiety.* Nat Neurosci, 2015. **18**(10): p. 1394-404.
12. Adhikari, A., M.A. Topiwala, and J.A. Gordon, *Synchronized Activity between the Ventral Hippocampus and the Medial Prefrontal Cortex during Anxiety.* Neuron, 2010. **65**(2): p. 257-269.
13. Adhikari, A., M.A. Topiwala, and J.A. Gordon, *Single units in the medial prefrontal cortex with anxiety-related firing patterns are preferentially influenced by ventral hippocampal activity.* Neuron, 2011. **71**(5): p. 898-910.
14. Seidenbecher, T., et al., *Amygdalar and hippocampal theta rhythm synchronization during fear memory retrieval.* Science, 2003. **301**(5634): p. 846-50.
15. Dzirasa, K., et al., *Impaired limbic gamma oscillatory synchrony during anxiety-related behavior in a genetic mouse model of bipolar mania.* J Neurosci, 2011. **31**(17): p. 6449-56.
16. Lee, A.T., et al., *VIP Interneurons Contribute to Avoidance Behavior by Regulating Information Flow across Hippocampal-Prefrontal Networks.* Neuron, 2019. **102**(6): p. 1223-1234 e4.
17. Jacinto, L.R., J.J. Cerqueira, and N. Sousa, *Patterns of Theta Activity in Limbic Anxiety Circuit Preceding Exploratory Behavior in Approach-Avoidance Conflict.* Front Behav Neurosci, 2016. **10**: p. 171.
18. Felix-Ortiz, A.C., et al., *BLA to vHPC inputs modulate anxiety-related behaviors.* Neuron, 2013. **79**(4): p. 658-64.
19. Felix-Ortiz, A.C., et al., *Bidirectional modulation of anxiety-related and social behaviors by amygdala projections to the medial prefrontal cortex.* Neuroscience, 2016. **321**: p. 197-209.
20. Jimenez, J.C., et al., *Anxiety Cells in a Hippocampal-Hypothalamic Circuit.* Neuron, 2018. **97**(3): p. 670-683 e6.
21. Kjaerby, C., et al., *Serotonin 1B Receptors Regulate Prefrontal Function by Gating Callosal and Hippocampal Inputs.* Cell Rep, 2016. **17**(11): p. 2882-2890.
22. Padilla-Coreano, N., et al., *Direct Ventral Hippocampal-Prefrontal Input Is Required for Anxiety-Related Neural Activity and Behavior.* Neuron, 2016. **89**(4): p. 857-66.
23. Padilla-Coreano, N., et al., *Hippocampal-Prefrontal Theta Transmission Regulates Avoidance Behavior.* Neuron, 2019. **104**(3): p. 601-610 e4.
24. Walder-Christensen, K., et al., *Electome network factors: Capturing emotional brain networks related to health and disease.* Cell Rep Methods, 2024. **4**(1): p. 100691.
25. Talbot, A., et al., *Estimating a brain network predictive of stress and genotype with supervised autoencoders.* J R Stat Soc Ser C Appl Stat, 2023. **72**(4): p. 912-936.

26. Mague, S.D., et al., *Brain-wide electrical dynamics encode individual appetitive social behavior.* Neuron, 2022. **110**(10): p. 1728-1741 e7.
27. Hultman, R., et al., *Brain-wide Electrical Spatiotemporal Dynamics Encode Depression Vulnerability.* Cell, 2018. **173**(1): p. 166-180 e14.
28. Marcinkiewcz, C.A., et al., *Serotonin engages an anxiety and fear-promoting circuit in the extended amygdala.* Nature, 2016. **537**(7618): p. 97-101.
29. Cunniff, M.M., et al., *Altered hippocampal-prefrontal communication during anxiety-related avoidance in mice deficient for the autism-associated gene Pogz.* Elife, 2020. **9**.
30. Caruana, R., *Multitask Learning.* Machine Learning, 1997. **28**: p. 41–75.
31. Jackson, A.D., et al., *Amygdala-hippocampus somatostatin interneuron beta-synchrony underlies a cross-species biomarker of emotional state.* Neuron, 2024. **112**(7): p. 1182-1195 e5.
32. Berg, L., J. Eckardt, and O.A. Masseck, *Enhanced activity of pyramidal neurons in the infralimbic cortex drives anxiety behavior.* PLoS One, 2019. **14**(1): p. e0210949.
33. Gunaydin, L.A., et al., *Natural neural projection dynamics underlying social behavior.* Cell, 2014. **157**(7): p. 1535-51.
34. Maestas-Olguin, C., J.W. Fennelly, and N.S. Pentkowski, *Chemogenetic inhibition of ventral hippocampal CaMKIIalpha-expressing neurons attenuates anxiety- but not fear-like defensive behaviors in male Long-Evans hooded rats.* Neurosci Lett, 2021. **751**: p. 135777.
35. Association, A.P., *Diagnostic and statistical manual of mental disorders*. 5th ed., text rev ed. 2022.
36. Kessler, R.C., et al., *Anxious and non-anxious major depressive disorder in the World Health Organization World Mental Health Surveys.* Epidemiol Psychiatr Sci, 2015. **24**(3): p. 210-26.
37. Roybal, K., et al., *Mania-like behavior induced by disruption of CLOCK.* Proc Natl Acad Sci U S A, 2007. **104**(15): p. 6406-11.
38. King, D.P., et al., *Positional cloning of the mouse circadian clock gene.* Cell, 1997. **89**(4): p. 641-53.
39. Dzirasa, K., et al., *Lithium ameliorates nucleus accumbens phase signaling dysfunction in a genetic mouse model of mania.* J Neurosci, 2010. **30**(48): p. 16314 –16323.
40. Logan, R.W., et al., *Valproate reverses mania-like behaviors in mice via preferential targeting of HDAC2.* Mol Psychiatry, 2021. **26**(8): p. 4066-4084.
41. Krishnan, V., et al., *Molecular adaptations underlying susceptibility and resistance to social defeat in brain reward regions.* Cell, 2007. **131**(2): p. 391-404.
42. Berton, O., et al., *Essential role of BDNF in the mesolimbic dopamine pathway in social defeat stress.* Science, 2006. **311**(5762): p. 864-8.
43. Morel, C., et al., *Midbrain projection to the basolateral amygdala encodes anxiety-like but not depression-like behaviors.* Nat Commun, 2022. **13**(1): p. 1532.
44. Zhong, P., et al., *HCN2 channels in the ventral tegmental area regulate behavioral responses to chronic stress.* Elife, 2018. **7**.
45. Monteiro, S., et al., *An efficient chronic unpredictable stress protocol to induce stress-related responses in C57BL/6 mice.* Front Psychiatry, 2015. **6**: p. 6.
46. Golden, S.A., et al., *A standardized protocol for repeated social defeat stress in mice.* Nat Protoc, 2011. **6**(8): p. 1183-91.
47. Tsankova, N.M., et al., *Sustained hippocampal chromatin regulation in a mouse model of depression and antidepressant action.* Nat Neurosci, 2006. **9**(4): p. 519-25.
48. Dzirasa, K., et al., *Chronic in vivo multi-circuit neurophysiological recordings in mice.* J Neurosci Methods, 2011. **195**(1): p. 36-46.
49. Carlson, D., et al., *Dynamically Timed Stimulation of Corticolimbic Circuitry Activates a Stress-Compensatory Pathway.* Biol Psychiatry, 2017. **82**(12): p. 904-913.

50. Grossman, Y., et al., *A widespead oscillatory network encodes an aggressive internal state.* BioRxiv, 2024.
51. Geweke, J., *Measurement of Linear Dependence and Feedback between Multiple Time Series. .* Journal of the American Statistical Association, 1982. **77**: p. 304–313.
52. Barnett, L. and A.K. Seth, *The MVGC multivariate Granger causality toolbox: a new approach to Granger-causal inference.* J Neurosci Methods, 2014. **223**: p. 50-68.
53. Crawley, J.N., *What's Wrong With My Mouse?: behavioral phenotyping of transgenic and knockout mice*. Second ed. 2007, Hoboken, New Jersey: John Wiley & Sons, Inc.
54. Sweis, B.M., et al., *Sensitivity to "sunk costs" in mice, rats, and humans.* Science, 2018. **361**(6398): p. 178-181.
55. Durand-de Cuttoli, R., et al., *Distinct forms of regret linked to resilience versus susceptibility to stress are regulated by region-specific CREB function in mice.* Sci Adv, 2022. **8**(42): p. eadd5579.
56. Kumar, S., et al., *Cortical Control of Affective Networks.* J Neurosci, 2013. **33**(3): p. 1116 –1129.
57. Hultman, R., et al., *Dysregulation of Prefrontal Cortex-Mediated Slow-Evolving Limbic Dynamics Drives Stress-Induced Emotional Pathology.* Neuron, 2016. **91**(2): p. 439-52.
58. Kumar, S., et al., *Prefrontal cortex reactivity underlies trait vulnerability to chronic social defeat stress.* Nat Commun, 2014. **5**: p. 4537.
59. Kuhn, H.W., *The Hungarian method for the assignment problem.* Naval Research Logistics Quarterly, 1955. **2**(1-2): p. 83-97.
60. Zhou, P., et al., *Towards theoretically understanding why SGD generalizes better than ADAM in deep learning.* Proceedings of the 34th International Conference on Neural Information Processing Systems, 2020. **20**: p. 21285–21296.

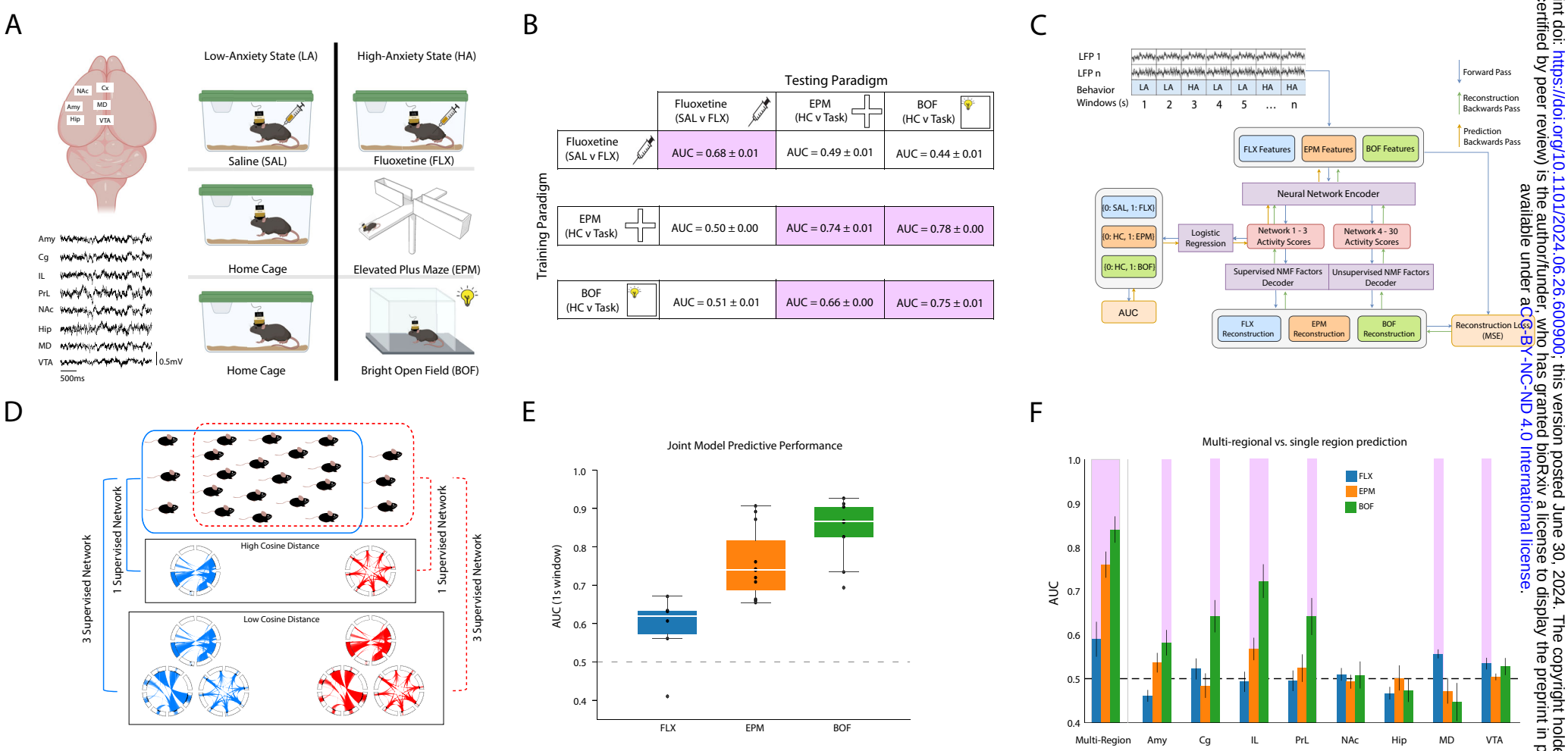

Figure 1

A

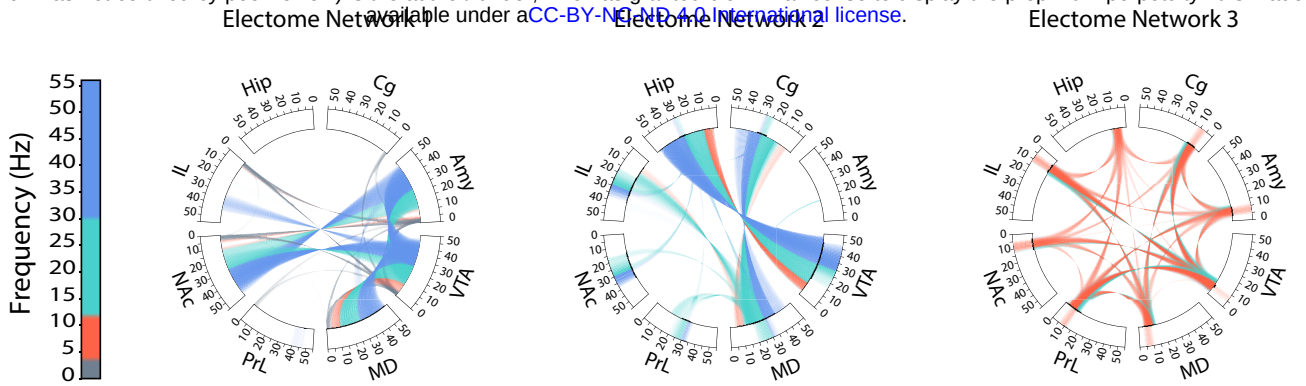

B

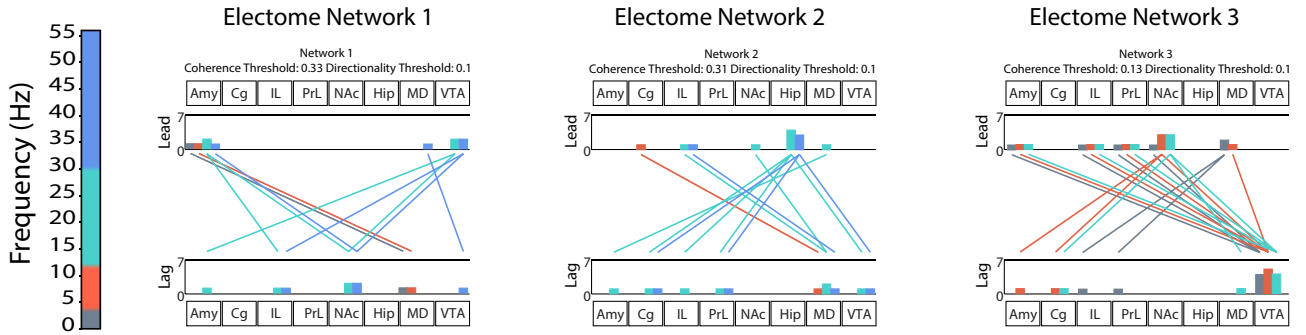

C

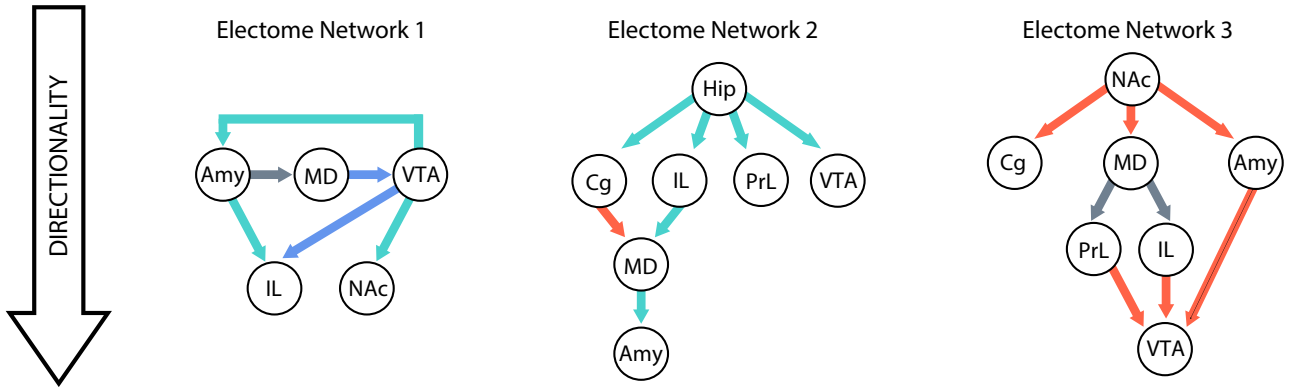

D

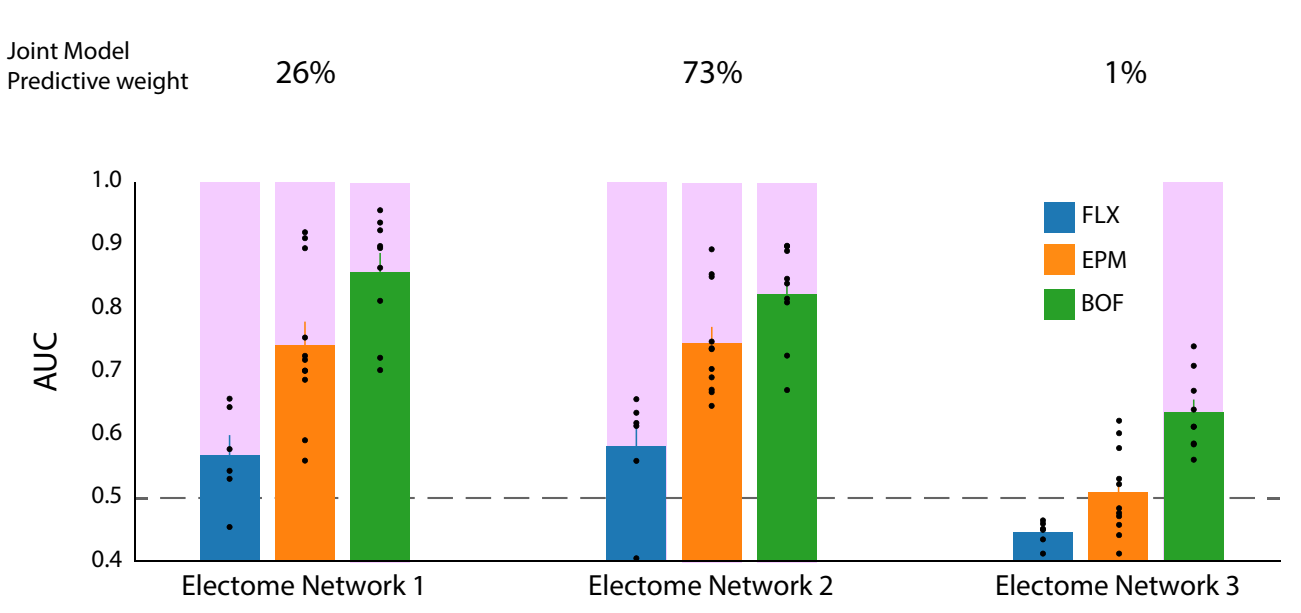

Figure 2

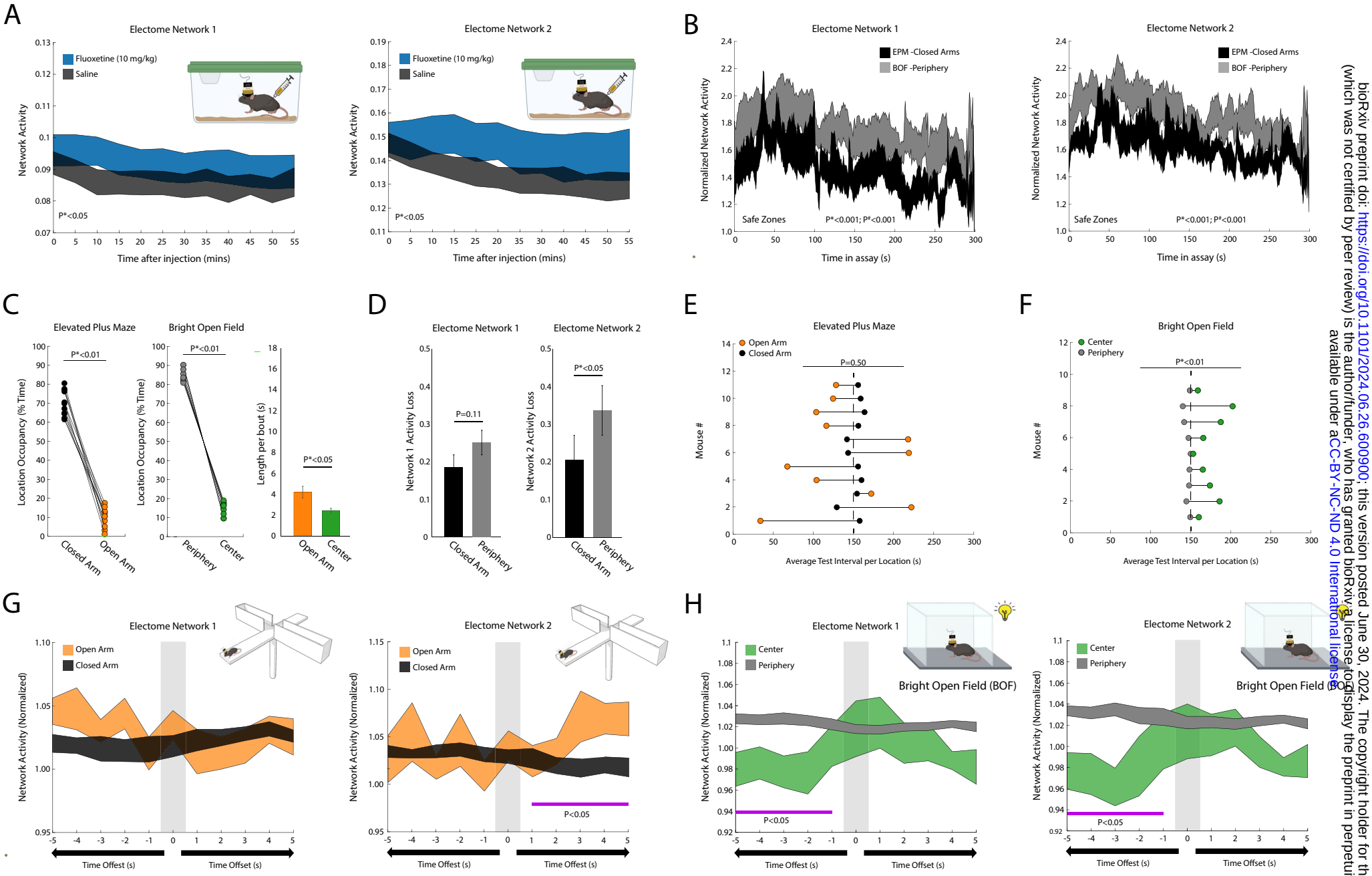

Figure 3

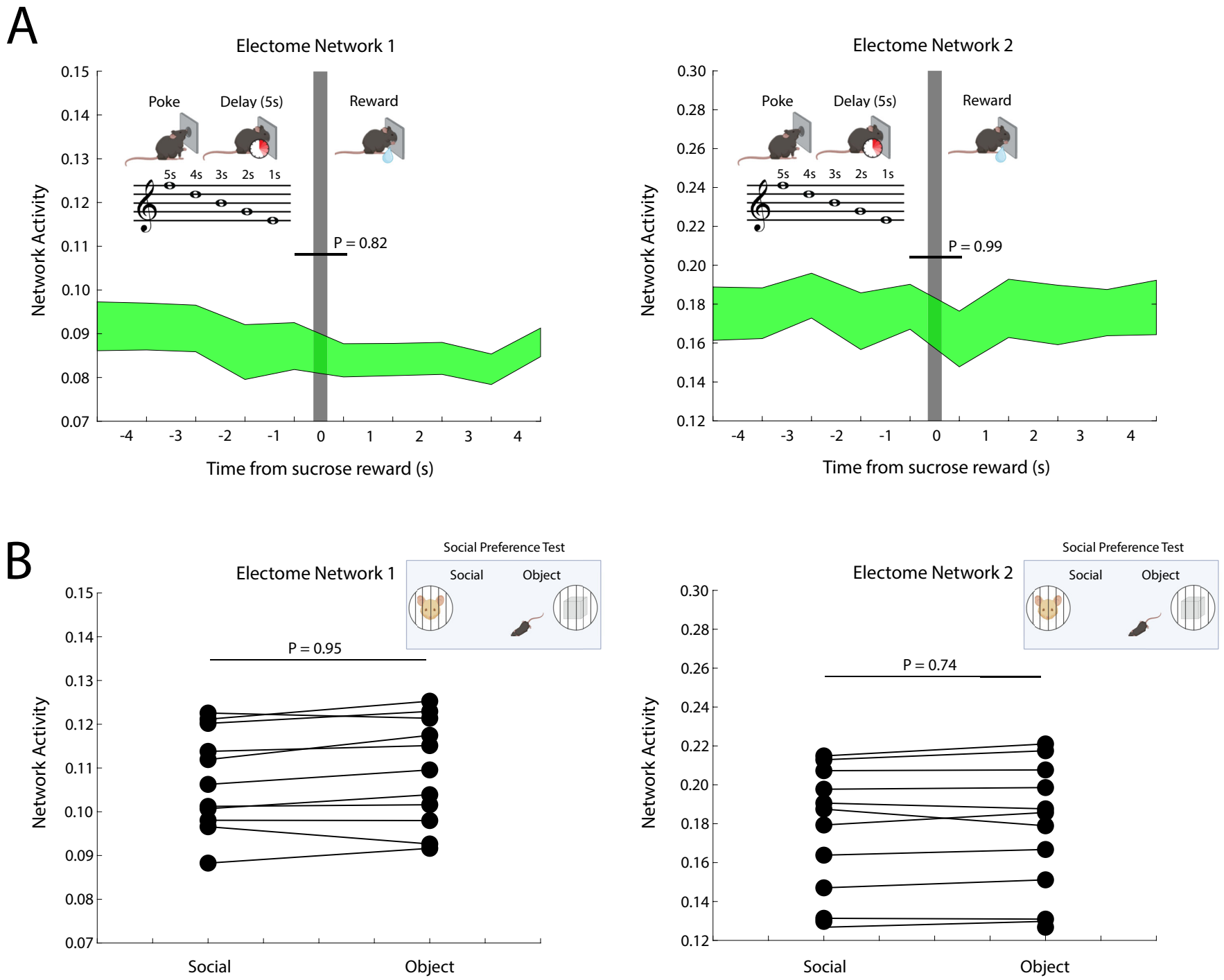

Figure 4

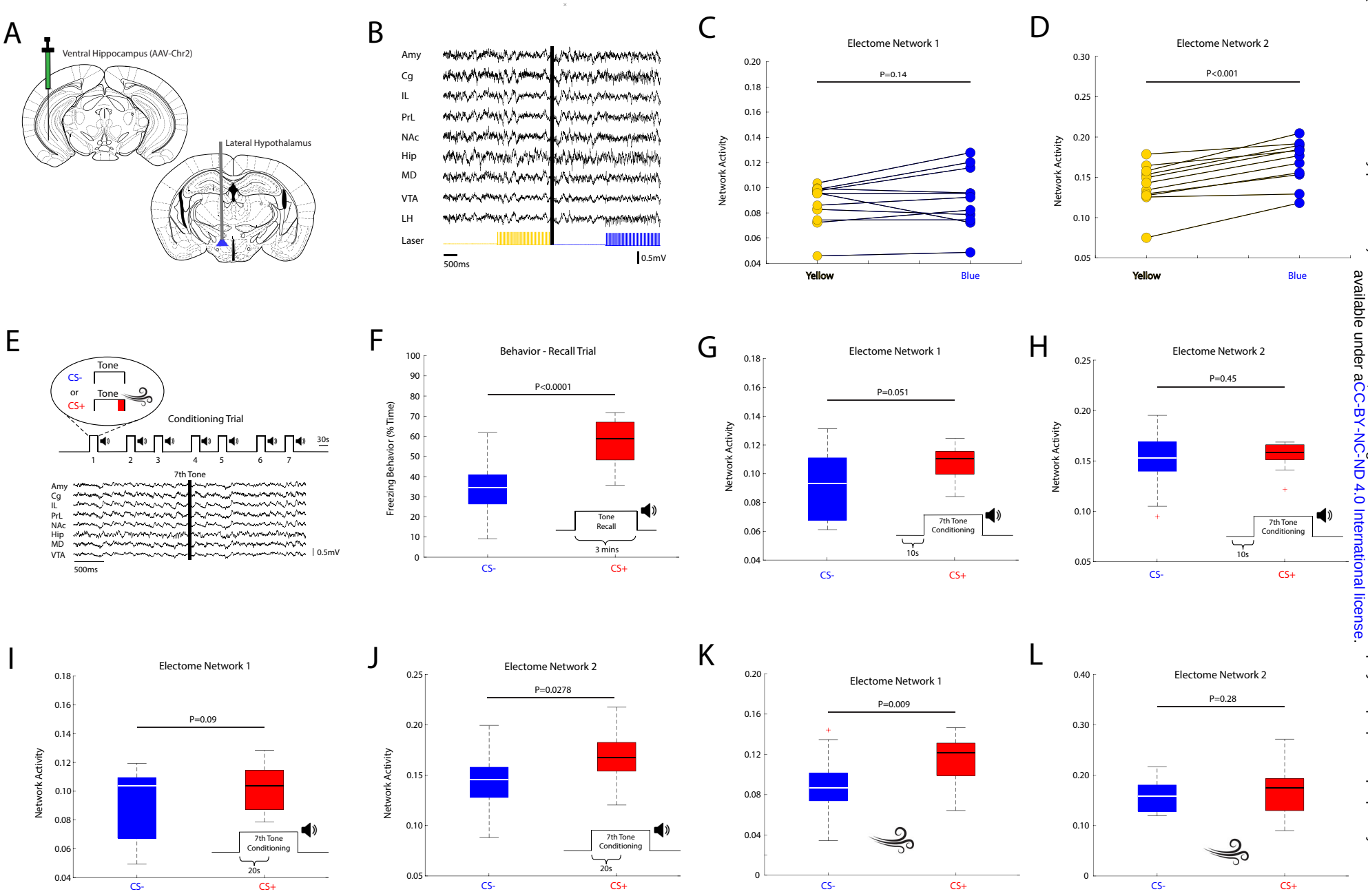

Figure 5

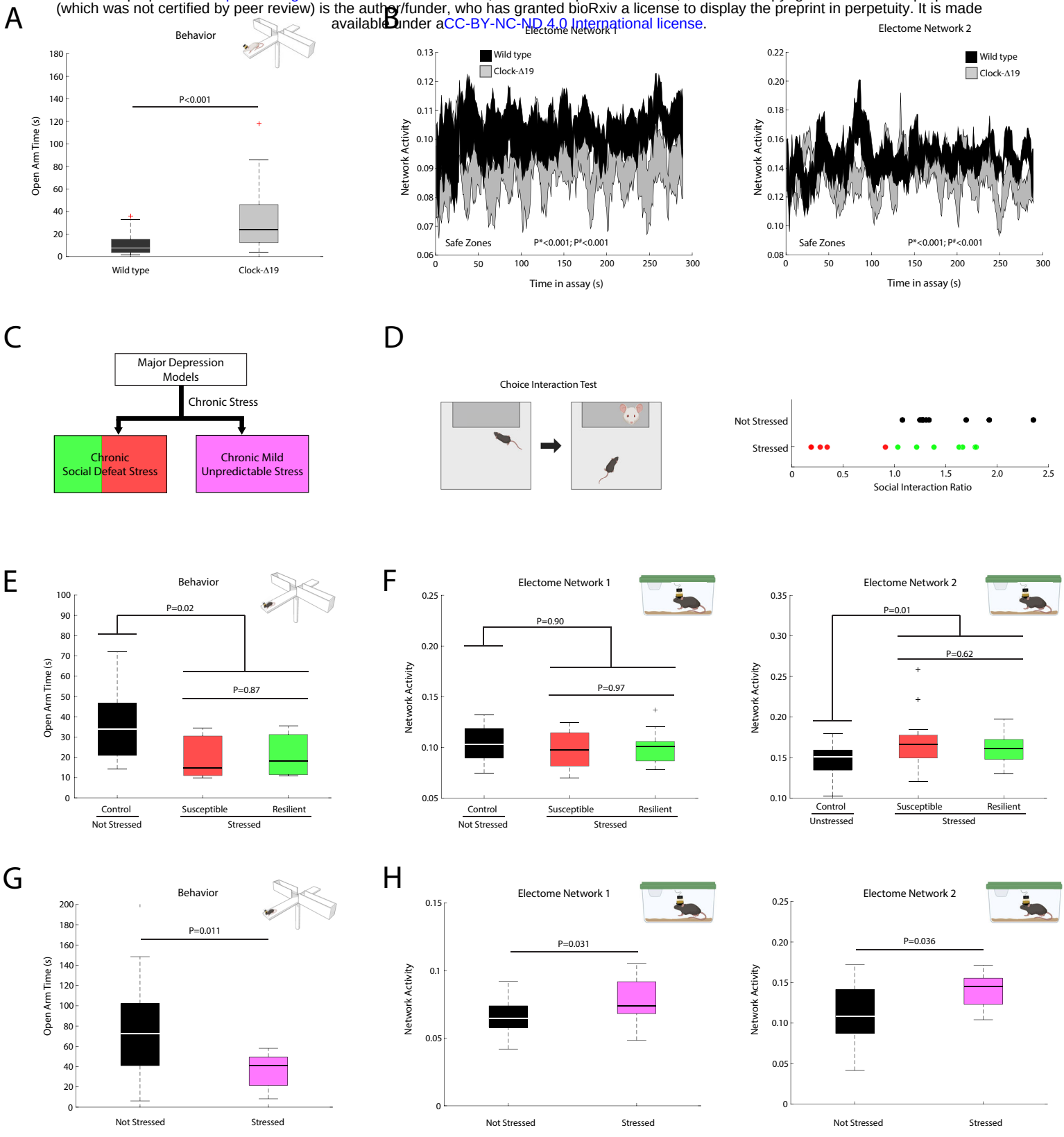

Figure 6

A

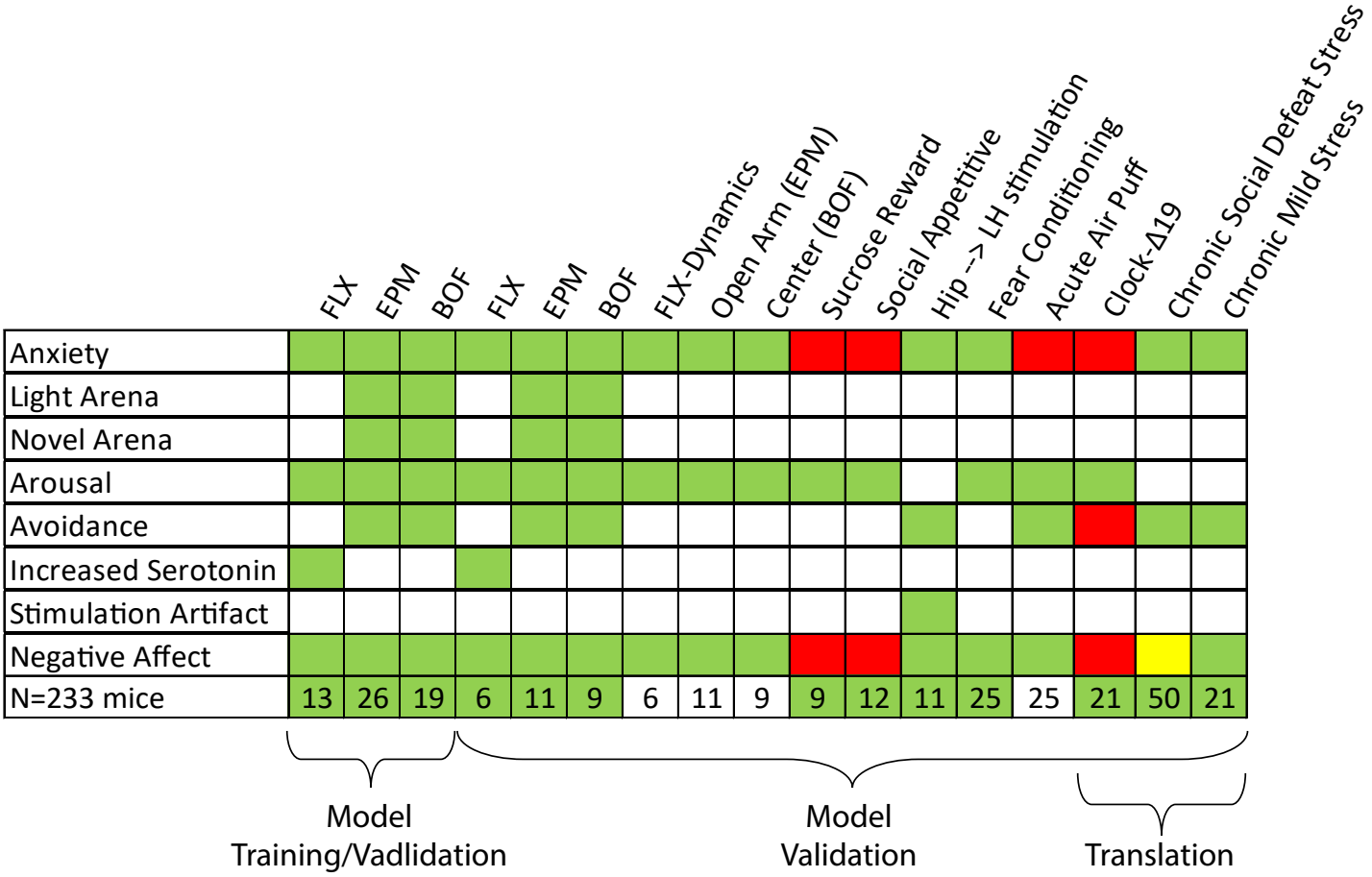

B

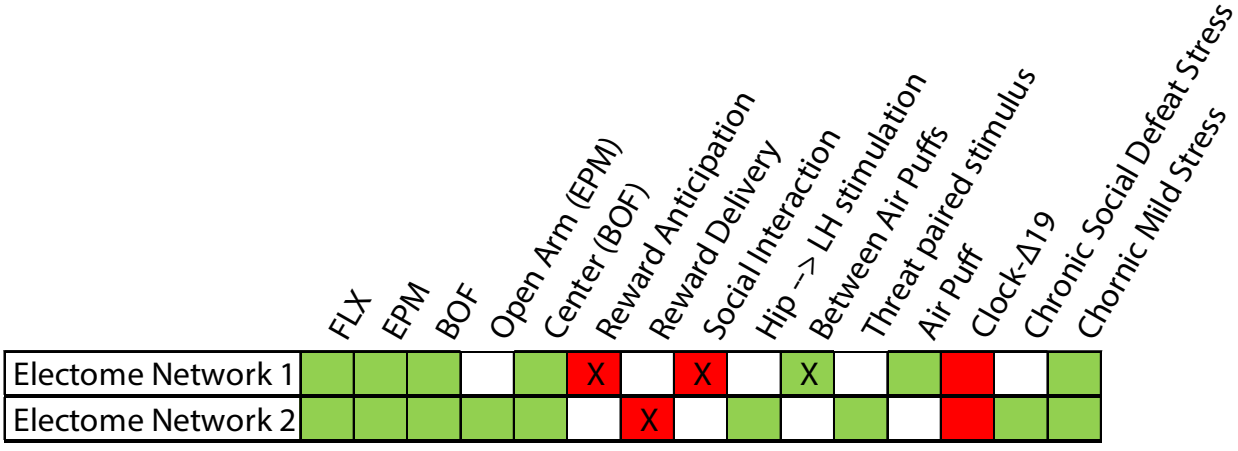

Figure 7